Doctoral Thesis

Gravitational lensing in a strong gravity region around a compact object

---

Supervisor:
Prof. Hideki Asada

Submitted March 2025

Graduate School of
Science and Technology
Hirosaki University

Ryuya Kudo

Acknowledgement

I most gratefully aknowledge suprviser H. Asada for helpful advice and continuous encouragement. I would like to thank M. C. Werner and Y. Sendouda for useful discussion and invaluable advice. I would like to thank H. Yoshino, K. Nakao, and Y. Koga for useful discussion. I wish to thank to all members of our group at Hirosaki University. Last but not least, I thank my friends and family.

Abstract

To explore the gravitational lensing in the strong gravitational field, this thesis investigates a relationship between two very accurate gravitational lens equations: the Virbhadra-Ellis (VE) equation proposed by [K. S. Virbhadra and G. F. R. Ellis, Phys. Rev. D 62, 084003 (2000)] and the Ohanian-Bozza (OB) equation improved by [V. Bozza, Phys. Rev. D 78, 103005 (2008)], based on a relation found by [H. C. Ohanian, Am. J. Phys. 55, 428 (1987)]. The VE equation is applicable only when the angular source position β is sufficiently small, and the angular diameter distances between the observer and the lens, D_L, and between the lens and the source plane, D_{LS}, are nearly equal to each other. In contrast, the OB equation remains valid even for large β and does not require the equidistance assumption.

One of the main results of this thesis is that the VE equation includes an unphysical branch, and the VE equation is improved by excluding this branch. It is found that the VE equation becomes a quadratic equation in $\tan\theta$ when the addition formula for tan is used. On the other hand, the OB equation can be transformed into a linear equation in $\tan\theta$ in the similar manner. This indicates that the VE equation contains spurious solutions that do not correspond to the lens diagram. By factorizing the VE equation, we find that the VE equation has two branches: plus branch and minus branch. We demonstrate that the minus branch has no solution corresponding to a lensed image. Thus, the minus branch is unphysical, and the improved VE equation is defined as the plus branch of the VE equation. In fact, it is shown that the plus branch of the VE equation reduces to the lens equation in the weak-field limit under the small-angle approximation.

Another main point is the derivation of a transformation formula between deflection angles defined differently for the improved VE equation and the OB equation. This result implies that the VE equation, which is previously applicable only for a small angular source position β, can be used even for large β. In addition, we model Sgr A^* as a Schwarzschild black hole lens to perform numerical computations. Numerical calculations further indicate that the proposed transformation formula for the deflection angle should be used, particularly when D_L/D_{LS} is sufficiently small.

As future work, it would be interesting to extends to stationary and axisym-

metric spacetimes along this study.

Contents

Publication List

1. **"Correspondence between two gravitational lens equations in a static and spherically symmetric spacetime"**
   R. Kudo and H. Asada
   Phys. Rev. D **111**, 044014 (2025).

2. **"Nondivergent deflection of light around a photon sphere of a compact object"**
   R. Kudo and H. Asada
   Phys. Rev. D **105**, 084014 (2022).

Chapter 1

Introduction

Gravitational lensing is a general term for phenomena involving electromagnetic waves propagating through a gravitational field, which are typically described in terms of light rays. In most of astronomical or cosmological situations, the light rays emitted from a distant source (e.g., a star, galaxy, or quasar) are deflected by the gravitational field of a massive object (e.g., a star, galaxy, or black hole) before reaching the observer. The first observed example of gravitational lensing occurred in 1919 [19], when Eddington and his collaborators confirmed Einstein's general relativity prediction regarding the deflection of starlight by the gravity of Sun. Since this observation, the gravitational lensing has been used as a powerful tool in modern astrophysics and gravitational physics, offering several key insights into the universe [12, 18, 50, 52, 70]:

1. **Probing Dark Matter**: Gravitational lensing allows us to map the distribution of dark matter, which does not interact with electromagnetic fields. By observing how light from distant objects is bent by an unseen mass, we can infer the presence and distribution of dark matter in galaxies, galaxy clusters and an intergalactic space.

2. **Measuring Cosmic Distances**: It enables precise measurements of the distances to distant galaxies and quasars, helping to improve our understanding of the large-scale structure of the universe and contributing to refining models of cosmic expansion.

3. **Detecting Exoplanets**: Microlensing, a specific type of gravitational lensing, can be used to detect exoplanets orbiting around distant stars. When a

foreground star passes in front of a background star, the resulting magnification can reveal planets orbiting around the lensing star.

4. **Testing General Relativity**: This phenomenon serves as a test of Einstein's general relativity on cosmic scales, to confirm its predictions regarding how massive objects bend the geometry of spacetime and affect the light traveling through it.

However, most of earlier works focused on the weak deflection of light.

A gravitational lens equation describes the mapping between the angular position of a source β and the angular position of the lensed image θ in terms of angular diameter distances [48, 50, 52]. In the weak gravitational field, the thin lens approximation is commonly used. This approximation simplifies the gravitational lens equation by assuming that the deflection of light occurs at a single plane, known as the lens plane, and that the distances between the observer, the lens, and the source are much larger than the deflection scale. The basic lens equation for weak gravitational lens is given by [52]

$$\beta = \theta - \frac{D_{LS}}{D_S}\alpha(\theta), \tag{1.1}$$

where D_S, D_L and D_{LS} are the angular diameter distances to the source, lens, and between the lens and source, respectively. The notion of the angular diameter distance is based on the intuitive idea that a distant object is smaller than it looks, accoding to the rule,

$$\text{object diameter} = \text{angle} \times \text{distance}.$$

$\alpha(\theta)$ represents the deflection angle of light. Eq. (1.1) works well for most astronomical situations, particularly when the gravitational field is relatively weak and the lensing object is not extremely compact.

In 2019 and 2022, the Event Horizon Telescope (EHT) team has succeeded in taking direct images of the immediate vicinity of the central black hole candidate of M87 galaxy and our galaxy [2, 3]. These observations have increased our renewed interest in the strong deflection of light in the strong gravitational field. In addition, the project of the next generation Event Horizon Telescope (ngEHT) is increasing the importance of the lens by strong gravity [4].

Exact (or very accurate) treatments of gravitational lensing are essential for both theoretical studies [5, 16, 47] and observational research in the strong gravity region. Since Virbhadra and Ellis's pioneering work, which proposed an very accurate gravitational lens equation in a static and spherically symmetric spacetime [66], significant progress has been made in understanding the behavior of

light rays in the strong gravitational field. Their formulation, although nearly exact [47], assumes that the deflection of light occurs in the lens plane, which is a good approximation when the observer, lens, and source are almost aligned.

By relaxing the assumption of almost alignment between the observer, lens, and source, Bozza has made use of the Ohanian relation for a more general configuration [44] to obtain an improved version of the accurate lens equation (For its simplicity, the improved equation is referred to as Ohanian-Bozza (OB) equation) [6]. Later, Takizawa, Ono, and Asada later rediscovered this equation using a formulation based on the Gauss-Bonnet theorem [22, 29, 30, 60].

With the development of the EHT and the direct imaging of black hole candidates, the need for more accurate treatments of gravitational lens equations near compact objects has become increasingly important. The VE equation has been widely used in discussions of gravitational lensing in SSS spacetimes. The OB equation seems to be very different from the VE equation, but is this really the case?

The main purpose of this thesis is to investigate the differences between the VE and OB equations and propose an improved version of the VE equation by removing its unphysical branches. We will then explore whether these two equations are fundamentally equivalent under specific transformations. Finally, we will discuss possible numerical differences when the transformation between the deflection angles is ignored.

This thesis is is organized as follows: In chapter 2, we provide some preliminaries for this thesis. In Section 2.1, we introduce the notation and necessary mathematical concepts used in this chapter. In Section 2.2, we provide a proof of Fermat's principle in a general spacetime (without imposing any specific symmetry) to discuss its application to the static and spherically symmetric spacetime considered in Subsection 2.4.2. We demonstrate that in static and spherically symmetric spacetimes, the problem can be analyzed in Euclidean space, similar to conventional optics. Section 2.3 addresses the definition of angular diameter distance. Finally, in Section 2.4, we describe static and spherically symmetric spacetimes and derive the equations for the deflection angle of light, which is used in the numerical calculations in Section 3.3 of Chapter 3. Capter 3 is the main part of this thesis. In this chapter, we discuss the differences between the VE and OB equations. Section 3.1 gives a brief review of two gravitational lens equations and discusses the unphysical branch in VE equation. Section 3.2 clarifies a relation between the improved VE equation and OB one and gives the expression for the transformation between the deflection angles in their formulation. Section 3.3 argues possible numerical differences when the deflection angle transformation is ignored. In chapter 4, we conclude the results of this thesis, and refer to future works.

Throughout this thesis, we will use the unit of $G = c = 1$.

Chapter 2

Preliminaries

In this chapter, we describe Fermat's principle which characterizes light rays propagating through a gravitational field, angular diameter distances, and equations used in the numerical calculations in Chapter 3. In Section 2.1, we introduce the notation and necessary mathematical concepts used in this chapter. In Section 2.2, we provide a proof of Fermat's principle in a general spacetime (without imposing any specific symmetry) to discuss its application to the static and spherically symmetric spacetime considered in Subsection 2.4.2. We demonstrate that in static and spherically symmetric spacetimes, light propagation in a spacetime can be analyzed in an Euclidean space, similar to conventional optics. Section 2.3 addresses the definition of angular diameter distance. Finally, in Section 2.4, we describe static and spherically symmetric spacetimes and derive the equations for the deflection angle of light, which is used in the numerical calculations in Section 3.3 of Chapter 3.

2.1 Notation and some notions

2.1.1 Notation and conventions

As is standard, we consider spacetime as a smooth 4-dimensional Lorentzian manifold equipped with a metric g, denoted as $(\mathcal{M}, g)$. We denote local coordinates on an open subset U of $\mathcal{M}$ as $\{x^\mu\}_{\mu=0,1,2,3}$, namely, for a local chart $\left(U, \varphi : \mathcal{M} \to \mathbb{R}^4\right)$ on $\mathcal{M}$, we set $x^\mu \equiv \mathbf{r}^\mu \circ \varphi \in \mathbb{R}$, where $\mathbf{r}^\mu : \mathbb{R}^4 \to \mathbb{R}$ denotes the projection function onto the μ-th coordinate axis of $\mathbb{R}^4$.

The tangent vector space at $p \in \mathcal{M}$ is denoted as $T_p\mathcal{M}$, and its coordinate basis is written as $\{\partial_\mu \equiv \partial/\partial x^\mu\}_{\mu=0,1,2,3}$. The disjoint union of the tangent vector spaces at all points $p \in \mathcal{M}$, $T\mathcal{M} \equiv \bigsqcup_{p\in\mathcal{M}} T_p\mathcal{M}$, is called the tangent bundle, where $\bigsqcup$ denotes the disjoint union. The set of all smooth section, $s : \mathcal{M} \to T\mathcal{M}$ such that $\pi \circ s = \mathrm{id}$, where $\pi : T\mathcal{M} \to \mathcal{M}$ is the natural projection onto $\mathcal{M}$ and id is the identity map, is the vector field on $\mathcal{M}$ denoted by $\Gamma(T\mathcal{M})$.

The Levi-Civita connection compatible with g is denoted as ∇, and its uniquely determined connection coefficients in the local coordinate system $\{x^\mu\}_{\mu=0,1,2,3}$ are given by

$$\Gamma^\mu_{\alpha\beta} = \frac{g^{\mu\lambda}}{2}\left(\partial_\alpha g_{\beta\lambda} + \partial_\beta g_{\alpha\lambda} - \partial_\lambda g_{\alpha\beta}\right),$$

which are called the Christoffel symbols.

The Riemann curvature tensor is denoted as Rm. For any vector fields $U, V, W \in \Gamma(T\mathcal{M})$, the Riemann tensor is defined as

$$\mathrm{Rm}(U,V)W \equiv \nabla_U\nabla_V W - \nabla_V\nabla_U W - \nabla_{[U,V]}W, \tag{2.1}$$

where $[\cdot,\cdot]$ denotes the Lie bracket on $\mathcal{M}$. If, in particular, $\{\partial_\mu\}$ is a coordinate basis, this has the coordinate version

$$\mathrm{Rm}_{\mu\nu\rho}{}^\lambda = \partial_\mu\Gamma^\lambda_{\nu\rho} - \partial_\nu\Gamma^\lambda_{\mu\rho} + \Gamma^\sigma_{\nu\rho}\Gamma^\lambda_{\mu\sigma} - \Gamma^\sigma_{\mu\rho}\Gamma^\lambda_{\nu\sigma}.$$

On a manifold $\mathcal{M}$ the Lie derivative L is a tensor derivation such that for any $V, X \in \Gamma(T\mathcal{M})$ and any smooth function f defined on $\mathcal{M}$ we have

$$L_V f = V(f),$$
$$L_V X = [V, X].$$

Now, we can define Killing vector fields. A Killing vector field on $\mathcal{M}$ is a vector field K for which the Lie derivative of the metric tensor vanishes, i.e., $L_K g = 0$. This equation, called Killing's equation, is equivalent to

$$g(\nabla_X K, Y) + g(\nabla_Y K, X) = 0, \tag{2.2}$$

for any $X, Y \in \Gamma(T\mathcal{M})$. Under the flow of a Killing vector field K, the metric tensor does not change. Therefore, a Killing vector field is an infinitesimal isometry. One of the most useful properties of Killing vector fields is the following: Let K be a Killing vector field and $\gamma : \mathcal{I} \to \mathcal{M}$ an affinly parametrized geodesic with tangent vector $\dot\gamma = d\gamma/dv$. Then $g(K, \dot\gamma)$ is constant along γ. By straightfoward calculation, we can show this statement:

$$\frac{d}{dv}g(K,\dot\gamma) = g(\nabla_{\dot\gamma}K, \dot\gamma) + \frac{1}{2}g(K, \nabla_{\dot\gamma}\dot\gamma) = 0, \tag{2.3}$$

since the first term vanishes by Killing's equation (2.2) and the second term vanishes the geodesic equation.

2.1.2 Variation of a smooth curve and variation vector fields

To prove Fermat's principle in Section 2.2 and define the angular diameter distance in Section 2.3, we need to consider small deformations of null curves. To describe this, we first introduce the concept of a variation of a general curve.

Let $\mathcal{N} = [0,1] \times (-\varepsilon_0, \varepsilon_0)$ be a subset of the two-dimensional real space $\mathbb{R}^2$. A variation η of a smooth curve $\gamma : [0,1] \to \mathcal{M}$ in spacetime $(\mathcal{M}, g)$ is a differentiable mapping

$$\eta : \mathcal{N} \to \mathcal{M}; \quad (v, \varepsilon) \mapsto \eta(v, \varepsilon), \tag{2.4}$$

such that, for all $v \in [0,1]$,

$$\eta(v, 0) = \gamma(v).$$

Here, ε_0 is a suitably chosen positive constant. See Figure 2.1. In other words, fixing $\varepsilon \in (-\varepsilon_0, \varepsilon_0)$, the mapping

$$\gamma_\varepsilon(v) \equiv \eta(v, \varepsilon)$$

represents a curve in $\mathcal{M}$ with $\gamma_0(v) = \gamma(v)$, where ε serves as a parameter labeling each curve. The family of curves obtained by smoothly varying ε,

$$\{\gamma_\varepsilon(v)\}_{\varepsilon \in (-\varepsilon_0, \varepsilon_0)},$$

is called a family of curves. For simplicity, we denote this family as $\{\gamma_\varepsilon\}$.

The standard coordinates of $\mathcal{N}$ are expressed as $(y^1, y^2) = (v, \varepsilon)$. Let the natural coordinate basis of $\mathcal{N}$ be $\partial_1 \equiv \partial_v$ and $\partial_2 \equiv \partial_\varepsilon$. Then, η induces tangent vectors on $T_{\eta(v,\varepsilon)}\mathcal{M}$ as

$$X_i \equiv \eta_*(\partial_i), \quad (i = 1, 2), \quad X_1 = X_v, \quad X_2 = X_\varepsilon, \tag{2.5}$$

where

$$\eta_* : T_{(v,\varepsilon)}\mathcal{N} \to T_{\eta(v,\varepsilon)}\mathcal{M}$$

is the differential map (also called the pushforward) induced by η. For any smooth function $f : \mathcal{M} \to \mathbb{R}$, the action of $\eta_*(\partial_i)$ is defined as

$$(\eta_*(\partial_i))(f) \equiv \partial_i (f \circ \eta).$$

The local coordinate representation of X_i is given by

$$X_v^\mu = \frac{\partial \eta^\mu}{\partial v}(v, \varepsilon), \quad X_\varepsilon^\mu = \frac{\partial \eta^\mu}{\partial \varepsilon}(v, \varepsilon), \quad (\mu = 0, 1, 2, 3), \tag{2.6}$$

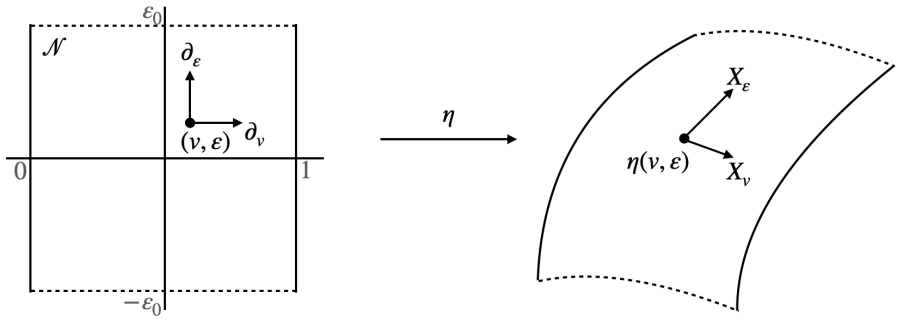

Figure 2.1: Schematic figure of the variation of a smoothe curve γ.

where $\eta^\mu = \mathbf{r}^\mu \circ \psi \circ \eta \in \mathbb{R}$.

An important relation involving the vector fields $X_i,\ (i = 1, 2)$ is

$$[X_v, X_\varepsilon] = \nabla_{X_\varepsilon} X_v - \nabla_{X_v} X_\varepsilon = 0, \tag{2.7}$$

which can be shown through a direct computation in the local coordinates $\{x^\mu = \eta^\mu\}$:

$$\begin{aligned} X_\varepsilon^\nu \nabla_\nu X_v^\mu &= X_\varepsilon^\nu \left(\partial_\nu X_v^\mu + \Gamma^\mu_{\nu\lambda} X_v^\lambda\right) \\ &= \partial_\varepsilon \partial_v \eta^\mu + \Gamma^\mu_{\nu\lambda} \left(\partial_\varepsilon \eta^\nu\right) \left(\partial_v \eta^\lambda\right) \\ &= \partial_v \partial_\varepsilon \eta^\mu + \Gamma^\mu_{\nu\lambda} \left(\partial_v \eta^\nu\right) \left(\partial_\varepsilon \eta^\lambda\right) \\ &= X_v^\nu \nabla_\nu X_\varepsilon^\mu. \end{aligned}$$

The step from the first to the second equality uses the local coordinate representation of X_i, while the step from the second to the third equality uses the symmetry of the Christoffel symbols with respect to the lower two indices.

We define the energy integral to prove Fermat's principle in Section 2.2. For a smooth curve $\gamma : [0, 1] \to \mathcal{M}$ in $\mathcal{M}$, the energy integral is defined as the line integral

$$\mathcal{S}[\gamma] = \frac{1}{2} \int_0^1 g\left(\dot\gamma(v), \dot\gamma(v)\right) dv, \tag{2.8}$$

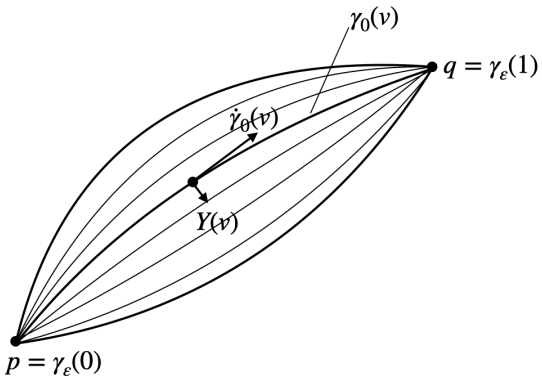

Figure 2.2: Variations with fixed endpoints and the variation vectors. The curve $\gamma(v)$ is smoothly deformed into a family of curves $\gamma_\varepsilon(v)$ parameterized by ε. At each point along γ, the variation vector $Y(v)$ represents the infinitesimal displacement of γ_ε with respect to ε.

where $\dot{\gamma}(v) = (d/dv)\gamma(v)$. This integral is referred to as the energy integral along the curve γ. It corresponds to the action of a free particle in the Lagrangian formalism.

We examine how the value of $\mathcal{S}[\gamma]$ changes when the curve $\gamma(v)$ is slightly deformed. To do so, we first define the notion of a variation vector along the curve. A variation vector is defined as follows: Given a variation

$$\eta : \mathcal{N} = [0,1] \times (-\varepsilon_0, \varepsilon_0) \to \mathcal{M}$$

of the curve $\gamma : [0,1] \to \mathcal{M}$, the *variation vector* $Y(v)$ along $\gamma(v)$ is given by

$$Y(v) \equiv X_\varepsilon(v,0), \tag{2.9}$$

where $X_\varepsilon = \eta_*(\partial_\varepsilon)$ is the pushforward of the coordinate vector field ∂_ε induced by η (See Figure 2.2).

It is important to note that $\dot{\gamma}(v)$ and $Y(v)$ are the values of the vector fields $\dot{\gamma}$ and Y, respectively, at the point $\gamma(v)$ on the curve γ. The *variation vector field* Y is an element of $\Gamma(T\mathcal{M})$, the space of smooth sections of the tangent bundle $T\mathcal{M}$.

2.1.3 Jacobi fields

Let $\gamma : [0,1] \to \mathcal{M}$ be a geodesic in a four-dimensional spacetime and let $\eta : [0,1] \times (-\varepsilon_0, \varepsilon_0) \to \mathcal{M}$ be its variation. We consider variations such that each curve in the family $\{\gamma_\varepsilon\}$ is a geodesic. The geodesic equation for $\gamma_\varepsilon(v)$ is given by

$$\nabla_{\dot{\gamma}_\varepsilon(v)} \dot{\gamma}_\varepsilon(v) = \nabla_{X_v} X_v = 0.$$

Using this, we derive

$$\begin{aligned} \nabla_{X_v} \left(\nabla_{X_v} X_\varepsilon \right) &= \nabla_{X_v} \left(\nabla_{X_\varepsilon} X_v \right) = \nabla_{X_\varepsilon} \left(\nabla_{X_v} X_v \right) + \mathrm{Rm}(X_v, X_\varepsilon) X_v \\ &= \mathrm{Rm}(X_v, X_\varepsilon) X_v. \end{aligned}$$

Evaluating the above equation at $\varepsilon = 0$, we obtain the equation for the variation vector $Y(v)$:

$$\nabla_{\dot{\gamma}(v)} \left(\nabla_{\dot{\gamma}(v)} Y(v) \right) = \mathrm{Rm} \left(\dot{\gamma}(v), Y(v) \right) \dot{\gamma}(v), \tag{2.10}$$

where Rm is the Riemannian curvature tensor defined in Eq. (2.1). This equation is known as the *Jacobi equation* or the geodesic deviation equation. Among the variation vector fields Y along the geodesic γ, those satisfying the Jacobi equation (2.10) are called *Jacobi fields* along γ.

Now, consider the case where each curve $\gamma_\varepsilon(v)$ in the family $\{\gamma_\varepsilon\}$ is a null geodesic. For each $\varepsilon \in (-\varepsilon_0, \varepsilon_0)$, we have

$$g \left(\dot{\gamma}_\varepsilon(v), \dot{\gamma}_\varepsilon(v) \right) = g \left(X_v, X_v \right) = 0.$$

Moreover, assuming that null geodesics are emitted from a point p_S in $\mathcal{M}$, the variation vector at the starting point satisfies $Y(0) = 0$. Evaluating the derivative of the null condition with respect to ε, we find

$$\begin{aligned} 0 &= X_\varepsilon \left\{ g \left(X_v, X_v \right) \right\} \\ &= 2g \left(X_v, \nabla_{X_\varepsilon} X_v \right) = 2g \left(X_v, \nabla_{X_v} X_\varepsilon \right) \\ &= 2g \left(\dot{\gamma}_\varepsilon(v), \nabla_{\dot{\gamma}_\varepsilon(v)} X_\varepsilon \right). \end{aligned}$$

At $(v, \varepsilon) = (0, 0)$, this simplifies to

$$g \left(\dot{\gamma}(0), \nabla_{\dot{\gamma}(0)} Y(0) \right) = 0. \tag{2.11}$$

On the other hand, since γ is a geodesic, we compute the second derivative of

the scalar product of $Y(v)$ and $\dot{\gamma}(v)$:

$$\begin{aligned}\frac{d^2}{dv^2}g\left(Y(v),\dot{\gamma}(v)\right) &= \frac{d}{dv}\left\{g\left(\nabla_{\dot{\gamma}(v)}Y(v),\dot{\gamma}(v)\right)+g\left(Y(v),\nabla_{\dot{\gamma}(v)}\dot{\gamma}(v)\right)\right\}\\ &= \frac{d}{dv}g\left(\nabla_{\dot{\gamma}(v)}Y(v),\dot{\gamma}(v)\right) \quad \left(\because\ \nabla_{\dot{\gamma}(v)}\dot{\gamma}(v)=0\right)\\ &= g\left(\nabla_{\dot{\gamma}(v)}\nabla_{\dot{\gamma}(v)}Y(v),\dot{\gamma}(v)\right)\\ &= g\left(\mathrm{Rm}\left(\dot{\gamma}(v),Y(v)\right)\dot{\gamma}(v),\dot{\gamma}(v)\right) \quad (\because\ \text{Eq.(2.10)})\\ &= 0, \end{aligned} \tag{2.12}$$

where the final equality follows from the antisymmetry of the Riemann curvature tensor. Equation (2.12) implies that

$$G(v) \equiv g\left(Y(v),\dot{\gamma}(v)\right), \tag{2.13}$$

is a linear function of v. However, at the starting point p_S, $Y(0)=0$, which means

$$G(0) = g\left(Y(0),\dot{\gamma}(0)\right) = 0.$$

Moreover, Eq. (2.11) implies

$$\frac{dG}{dv}(0) = 0.$$

Thus, $G(v)$ must vanish along γ, and we conclude that

$$g\left(Y(v),\dot{\gamma}(v)\right) = 0, \tag{2.14}$$

holds along γ. This result shows that the Jacobi field Y is orthogonal to the null geodesic γ at every point along the curve.

2.2 Fermat's principle

Let $(\mathcal{M},g)$ be a four-dimensional spacetime. A null geodesic $\gamma:[0,1]\to\mathcal{M}$ with tangent vector $\dot{\gamma}=d\gamma/dv$ describes the path of a light ray (in vacuum). The null geodesic equation is given by

$$\nabla_{\dot{\gamma}}\dot{\gamma} = 0. \tag{2.15}$$

Alternatively, this can be derived as an extremal solution to the Euler-Lagrange equations for the Lagrangian

$$\mathcal{L}[\gamma] = \frac{1}{2}g(\dot{\gamma},\dot{\gamma}), \tag{2.16}$$

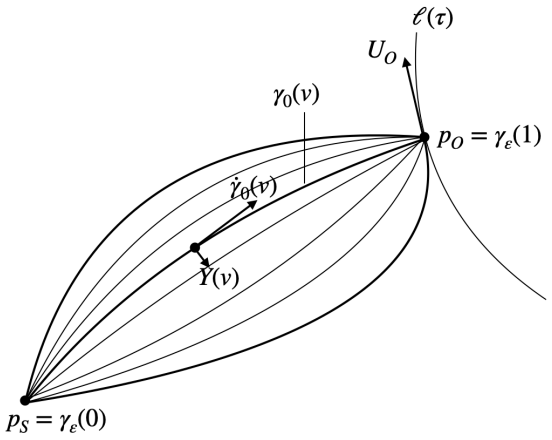

Figure 2.3: Geometry of Fermat's principle.

subject to the constraint $\mathcal{L} = 0$. This corresponds to the variational principle for the action (the energy integral defined in Section 2.1.3):

$$\delta S[\gamma] = \delta \int_0^1 \mathcal{L}[\gamma] dv = \delta \left\{ \frac{1}{2} \int_0^1 g(\dot{\gamma}, \dot{\gamma}) dv \right\} = 0. \tag{2.17}$$

However, an intuitive and practically useful way to characterize light rays, particularly in gravitational lensing (GL) theory, is provided by the following theorem [52].

Theorem (Fermat's principle): Let $(\mathcal{M}, g)$ be a four-dimensional spacetime. Let $p_S \in \mathcal{M}$ denote the emission event of a light source, and let $\ell : \mathcal{I} \to \mathcal{M}$ be a timelike worldline representing the observer, where $\mathcal{I}$ is a real interval. A null curve $\gamma : [0, 1] \to \mathcal{M}$ connecting p_S to ℓ is a null geodesic if and only if the arrival time τ at ℓ is stationary under first-order variations of γ among all smooth null curves connecting p_S to ℓ, i.e.,

$$\delta\tau = 0, \tag{2.18}$$

where $\delta(\cdot) \equiv \frac{d}{d\varepsilon}(\cdot)\big|_{\varepsilon=0}$.

Proof of Fermat's priciple: We proceed to prove Fermat's principle, where the proof presented here is based on the approach outlined in [52].

First, we assume that γ is a null geodesic and demonstrate that $\delta\tau = 0$. Let τ denote the proper time along the observer's worldline ℓ, with its tangent vector given by $\ell'(\tau) = d\ell/d\tau$. In a local coordinate system $\{\xi^\mu\}$, the components of $\ell'(\tau)$ are written as $d\xi^\mu(\tau)/d\tau$.

We adopt the notation for variations and variation vectors as introduced in Subsection 2.1.2. Specifically, the variation of the smooth curve γ and the variation vector $Y(s)$ are denoted as $\eta : [0,1] \times (-\varepsilon_0, \varepsilon_0) \to \mathcal{M}$, and $Y(v) = X_\varepsilon(v,0) = \eta_* (\partial_\varepsilon)|_{\varepsilon=0}$, respectively. Using this notation, we set $p_S = \eta(0,\varepsilon)$ and $\ell(\tau(\varepsilon)) = \eta(1,\varepsilon)$ (See Figure 2.3). Since the variation fixes the starting point p_S, the variation vector satisfies $Y(0) = 0$. At the endpoint $\ell(\tau(\varepsilon))$, we have

$$\begin{aligned} Y(1) = X_\varepsilon(1,0) &= \frac{d\xi^\mu(\tau(\varepsilon))}{d\varepsilon} \left(\frac{\partial}{\partial\xi^\mu}\right)_{\ell(\tau)} \Bigg|_{\varepsilon=0} \\ &= \frac{d\tau}{d\varepsilon}\frac{d\xi^\mu}{d\tau} \left(\frac{\partial}{\partial\xi^\mu}\right)_{\ell(\tau)} \Bigg|_{\varepsilon=0} \\ &= \ell'(\tau(0))\delta\tau, \end{aligned} \tag{2.19}$$

where $\delta\tau = \frac{d\tau}{d\varepsilon}\big|_{\varepsilon=0}$.

Next, consider a family of null curves $\{\gamma_\varepsilon(v) = \eta(v,\varepsilon)\}$ connecting p_S to ℓ, such that

$$g(\dot\gamma_\varepsilon(v), \dot\gamma_\varepsilon(v)) = g(X_v, X_v) = 0, \tag{2.20}$$

for all v and ε. Then,

$$\begin{aligned}
0 &= \delta \left\{ \frac{1}{2} \int_0^1 g(\dot{\gamma}_\varepsilon(v), \dot{\gamma}_\varepsilon(v)) dv \right\} \\
&= \frac{1}{2} \int_0^1 X_\varepsilon \left(g(X_v, X_v) \right)|_{\varepsilon=0} \, dv \\
&= \int_0^1 g(X_v, \nabla_{X_\varepsilon} X_v)|_{\varepsilon=0} \, dv \\
&= \int_0^1 g(X_v, \nabla_{X_v} X_\varepsilon)|_{\varepsilon=0} \, dv \\
&= \int_0^1 g(\dot{\gamma}, \nabla_{\dot{\gamma}} Y(v)) dv \\
&= \int_0^1 \left\{ \frac{d}{dv} \left(g(Y(v), \dot{\gamma}) \right) - g(\nabla_{\dot{\gamma}} \dot{\gamma}, Y(v)) \right\} dv \\
&= \left[g\left(Y(v), \dot{\gamma}\right) \right]_{v=0}^1 - \int_0^1 g(\nabla_{\dot{\gamma}} \dot{\gamma}, Y(v)) dv, \qquad (2.21)
\end{aligned}$$

where we used Eq. (2.7), $[X_v, X_\varepsilon] = 0$, obtained in Subsection 2.1.2 in the forth equality. The first term of Eq. (2.21) is computed as

$$\begin{aligned}
\left[g\left(Y(v), \dot{\gamma}(v)\right) \right]_{v=0}^1 &= g\left(Y(1), \dot{\gamma}(1)\right) - g\left(Y(0), \dot{\gamma}(0)\right) \\
&= g\left(\ell'(\tau(0)), \dot{\gamma}(1)\right) \delta\tau,
\end{aligned}$$

where we used $Y(0) = 0$ and Eq. (2.19).

Thus, Eq. (2.21) becomes

$$g\left(\ell'(\tau(0)), \dot{\eta}_0(1)\right) \delta\tau - \int_0^1 g(\nabla_{\dot{\gamma}} \dot{\gamma}, Y(v))|_{\varepsilon=0} \, dv = 0. \qquad (2.22)$$

Since both ℓ' and $\dot{\gamma}$ are the future-directed tangent vectors, i.e., $g\left(\ell'(\tau(1)), \dot{\eta}_0(1)\right) > 0$, and γ is a null geodesic, we conclude that

$$\delta\tau = 0. \qquad (2.23)$$

To prove the converse, we assume $\delta\tau = 0$ and show that γ is a null geodesic. To do this, we construct a variation vector field $Z(v)$.

First, we examine the conditions that the variation vector field $Z(v)$ must satisfy. The variation of the null condition,

$$g\left(\dot{\gamma}(v), \dot{\gamma}(v)\right) = 0, \qquad (2.24)$$

yields

$$\delta g\left(\dot{\gamma}(v), \dot{\gamma}(v)\right) = 2g\left(\dot{\gamma}(v), \nabla_{\dot{\gamma}(v)} Z(v)\right) = 0.$$

Thus, one condition for $Z(v)$ is

$$g\left(\dot{\gamma}(v), \nabla_{\dot{\gamma}(v)} Z(v)\right) = 0. \tag{2.25}$$

Additionally, $Z(v)$ must satisfy

$$Z(0) = 0, \quad Z(1) \propto \ell'(\tau(0)). \tag{2.26}$$

To construct $Z(v)$ satisfying two conditions (2.25) and (2.26), consider a vector field $U(v)$ along γ obtained by parallel transporting $\ell'(\tau(0))$ backward along γ. Note that by definition, $U(v)$ satisfies

$$\dot{U}(v) = \nabla_{\dot{\gamma}} U(v) = 0, \tag{2.27}$$

and $U(1) = \ell'(\tau(0))$. Next, introduce an arbitrary vector field $W(v)$ along γ such that

$$W(0) = W(1) = 0.$$

Using $U(v)$ and $W(v)$, construct the variation vector field $Z(v)$ as follows:

$$Z(v) \equiv W(v) - U(v) \int_0^v \frac{g\left(\dot{W}(\bar{v}), \dot{\gamma}(\bar{v})\right)}{g\left(U(\bar{v}), \dot{\gamma}(\bar{v})\right)} d\bar{v}. \tag{2.28}$$

To verify condition (2.25), we compute

$$\begin{aligned}
\dot{Z}(v) &= \nabla_{\dot{\gamma}(v)} Z(v) \\
&= \dot{W}(v) - U(v) \frac{g\left(\dot{W}(v), \dot{\gamma}(v)\right)}{g\left(U(v), \dot{\gamma}(v)\right)} - \dot{U}(v) \int_0^v \frac{g\left(\dot{W}(\bar{v}), \dot{\gamma}(\bar{v})\right)}{g\left(U(\bar{v}), \dot{\gamma}(\bar{v})\right)} d\bar{v} \\
&= \dot{W}(v) - U(v) \frac{g\left(\dot{W}(v), \dot{\gamma}(v)\right)}{g\left(U(v), \dot{\gamma}(v)\right)}, \quad \left(\because \ \dot{U}(v) = 0\right).
\end{aligned} \tag{2.29}$$

Thus,

$$\begin{aligned}
g\left(\dot{\gamma}(v), \dot{Z}(v)\right) &= g\left(\dot{\gamma}(v), \dot{W}(v)\right) - g\left(\dot{\gamma}(v), U(v)\right) \cdot \frac{g\left(\dot{W}(v), \dot{\gamma}(v)\right)}{g\left(U(v), \dot{\gamma}(v)\right)} \\
&= 0.
\end{aligned} \tag{2.30}$$

Condition (2.26) is also satisfied since

$$Z(1) = W(1) - U(1) \int_0^1 \frac{g\left(\dot{W}(v), \dot{\gamma}(v)\right)}{g\left(U(v), \dot{\gamma}(v)\right)} dv. \tag{2.31}$$

Given $\delta\tau = 0$, we compute

$$\begin{aligned} 0 &= \delta\tau \\ &= g\left(\ell'(\tau(0)), \ell'(\tau(0))\right) \delta\tau \quad \left(\because\ g\left(\ell'(\tau(0)), \ell'(\tau(0))\right) = -1\right) \\ &= -g\left(U(1), Z(1)\right). \end{aligned} \tag{2.32}$$

Since $U(1) \neq 0$, we must have $Z(1) = 0$. From the expression for $Z(1)$, this implies

$$\int_0^1 \frac{g\left(\dot{W}(v), \dot{\gamma}(v)\right)}{g\left(U(v), \dot{\gamma}(v)\right)} dv = 0. \tag{2.33}$$

Performing integration by parts and using the arbitrariness of $W(v)$ in the open interval $(0, 1)$, we conclude that

$$\frac{d}{dv}\left(\frac{\dot{\gamma}(v)}{g\left(U(v), \dot{\gamma}(v)\right)}\right) = 0.$$

Setting $\Gamma(v) \equiv 1/g\left(U(v), \dot{\gamma}(v)\right)$, this implies

$$\begin{aligned} 0 &= \frac{d}{dv}\left(\Gamma(v)\dot{\gamma}(v)\right) \\ &= \dot{\Gamma}(v)\dot{\gamma}(v) + \Gamma(v)\ddot{\gamma}(v), \\ \therefore \ddot{\gamma}(v) &= -\frac{\dot{\Gamma}(v)}{\Gamma(v)}\dot{\gamma}(v). \end{aligned}$$

This is the geodesic equation.

The proof of Fermat's principle is finished.

An application of Fermat's principle to static and spherically symmetric spacetimes is discussed in Subsection 2.4.2.

2.3 Angular diameter distance

In the gravitationl lens equations there usually appear the distances between observer-lens, observer-source plane, and lens-source plane. However, in spacetime, "distance" is not unique. Instead, sevral model-dependent distances have been defined, whose values can be determined only indrectly [48, 50, 52]. In this

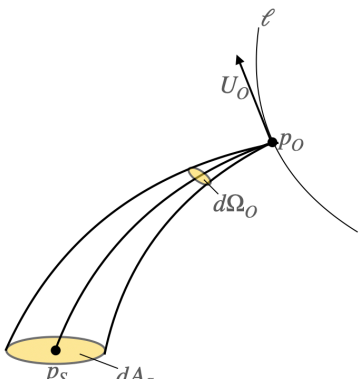

Figure 2.4: The family of light rays from the cross-sectional area dA_S of the source at p_S with vertex at the observer event p_O, of the size $d\Omega_O$, used to define the angular diameter distance of p_S from p_O.

subsection, we consider the angular diameter distance, commonly used in gravitational lensing theory, defined as follows.

The definition of the angular diameter distance is based on an intuitive idea:

$$\text{object diameter} \;=\; \text{angle} \;\times\; \text{distance}. \tag{2.34}$$

Formally, the angular diameter distance is defined as

$$D(p_S, U_O) \equiv \left(\frac{dA_S}{d\Omega_O}\right)^{1/2}, \tag{2.35}$$

where p_S is the source event, U_O is the 4-velocity of the observer at the event p_O, $d\Omega_O$ is the solid angle subtended by the source as seen by the observer, and dA_S is the physical cross-sectional area of the source. To ensure that the angular diameter distance is well-defined, we verify its consistency with the concepts and notations introduced in Subsection 2.1.2 and 2.1.3.

Using the notation introduced in Subsections 2.1.2 and 2.1.3, let $\gamma : [0,1] \to \mathcal{M}$ be a geodesic in a four-dimensional spacetime, and let $\eta : [0,1] \times (-\varepsilon_0, \varepsilon_0) \to \mathcal{M}$

be its variation. Consider a family of affinely parametrized null geodesics (light rays), $\{\gamma_\varepsilon\}$, with tangent vectors $\dot{\gamma}_\varepsilon(v)$. This family of curves represents the null geodesics connecting the source p_S and the observer p_O, satisfying $\gamma_\varepsilon(1) = p_S$ and $\gamma_\varepsilon(0) = p_O$. Note that, unlike before, the light rays are past-directed.

In this subsection, we set

$$k = X_v, \quad Y = X_\varepsilon. \tag{2.36}$$

From Eq. (2.7) in Subsection 2.1.2, it follows that

$$[k, Y] = \nabla_k Y - \nabla_Y k = 0. \tag{2.37}$$

Moreover, along the null geodesic γ, using Eq. (2.14) in Subsection 2.1.3, we have

$$g(k, Y) = 0. \tag{2.38}$$

From the discussion in Subsection 2.1.3, Y is a Jacobi field. In other words, Y satisfies the Jacobi equation (2.10):

$$\ddot{Y} = \mathrm{Rm}(k, Y)\, k, \tag{2.39}$$

where $\ddot{Y} \equiv \nabla_k \nabla_k Y$.

For the convenience, we introduce a Sachs basis $\{E_A\}_{A=1,2}$ such that

$$g(E_A, E_B) = \delta_{AB}, \quad g(k, E_A) = 0, \quad \nabla_k E_A = 0. \tag{2.40}$$

A sachs basis determines an observer's 4-vector field U_O at p_O with $g(U_O, U_O) = -1$ and $g(U_O, k) = 1$ along γ that perpendicular to E_1 and E_2. Ir is helpful to interpret this two-dimensional space as a screen. By construction, we therefore have

$$d\Omega_O = \det(g(E_A, E_B)) = 1. \tag{2.41}$$

in Eq.(2.35).

Now, we define an infinitesimally thin bundle along γ

$$\mathcal{B} = \left\{ c^A Y^A \,\middle|\, \delta_{AB} c^A c^B \leq 1 \right\}, \tag{2.42}$$

where c^A are some constants and Y_A are Jacobi fields. With respect to a Sachs basis, the basis vector fields Y_A of an infinitesimally thin bundle can be represented as

$$Y_A = J_A^B E_B + \epsilon_A k, \tag{2.43}$$

where ϵ_A are some constants and $\boldsymbol{J} = \left(J_A^B\right)$ relates the shape of the cross-section of the infinitesimally thin bundle of the Sachs basis. $\boldsymbol{J}$ is called the Jacobi matrix. Therefore, we can write dA_S in Eq. (2.35) as

$$dA_S = \det\left(g\left(Y_A, Y_B\right)\right) = \det \boldsymbol{J}. \tag{2.44}$$

We hence find that Eq. (2.35) is rewritten as

$$D_A = \sqrt{|\det \boldsymbol{J}|}, \tag{2.45}$$

which is well-defined geometrically.

However, in the case of gravitational lensing in a static and spherically symmetric spacetime, we can analyze graviational lnses by embedding into an Euclidean space (Section 2.4.2). Therefore, the discussion in Chapter 3 will be based on Eq. (2.34).

2.4 Gravitational lensing in a static and spherically symmetric spacetime

2.4.1 Static and spherically symmetric spacetime

First, we define a static spacetime. A spacetime $\mathcal{M}$ is said to be static if there exists a timelike Killing vector field ξ satisfying

$$\xi^\flat \wedge d\xi^\flat = 0, \tag{2.46}$$

where $\xi^\flat = g(\xi, \cdot) \in T^*\mathcal{M}$ is the 1-form dual to ξ, $\wedge$ denotes the wedge product, and d is the exterior derivative. The condition (2.46) implies, via Frobenius' theorem, that ξ is orthogonal to spatial hypersurfaces. In the absence of this condition, the spacetime is referred to as stationary.

The metric of any stationary spacetime, i.e., any metric possessing a timelike Killing vector field ξ, can locally be written as

$$g = A\left(dt + \hat{\phi}\right)^2 + h, \tag{2.47}$$

except at points where ξ vanishes. Here, $\xi = \partial_t$, implying $\partial_t g_{\mu\nu} = 0$. The function $A = g(\xi, \xi)$, and h is a Riemannian metric. With this form, we compute

$$\begin{aligned}
\xi^\flat &= -A\left(dt + \hat{\phi}\right), \\
d\xi^\flat &= -dA \wedge \left(dt + \hat{\phi}\right) - A d\hat{\phi}, \quad \left(\because\ d^2 = 0\right), \\
\xi^\flat \wedge d\xi^\flat &= -A\left(dt + \hat{\phi}\right) \wedge \left\{-dA \wedge \left(dt + \hat{\phi}\right) - A d\hat{\phi}\right\} \\
&= A^2\left(dt + \hat{\phi}\right) \wedge d\hat{\phi}.
\end{aligned}$$

This shows that g is static if and only if $d\hat{\phi} = 0$.

Therefore, for a static metric, there exists a function f such that $\hat{\phi} = df$. Introducing a new coordinate $\tau \equiv t + f$, we have $dt + df = d\tau$, and the static metric g can generally be written as

$$g = -Ad\tau^2 + h. \tag{2.48}$$

Moreover, Eq. (2.48) implies that the metric is invariant under the transformation $\tau \to -\tau$. Physically, this indicates that a static spacetime is also invariant under time reversal.

A spacetime is said to be spherically symmetric if its isometry group contains a subgroup isomorphic to $O(3)$ and the orbits of this subgroup are two-dimensional spheres, i.e., if in a local coordinate system $\left\{x^\mu = (t, x^i)\right\}$, where $i = 1, 2, 3$ represents the spatial components, for each $\psi \in \tilde{O}(3) \subset O(3)$, the map $(t, x^i) \to (t, \psi x^i)$ preserves distances and the set of transformed points forms a two-dimensional sphere. Physically, this implies that the spacetime metric is invariant under spatial rotations and thus a spherically symmetric spacetime is one whose metric remains invariant under rotations. Spherical symmetry suggests that the metric q on each orbit two-dimensional sphere must be a multiple of the metric on unit two-dimensional sphere $\mathbb{S}^2$. Thus q can be written as

$$q = B(r)dr^2 + C(r)\left(d\vartheta^2 + \sin^2\vartheta d\varphi^2\right). \tag{2.49}$$

By changing variable by $C(r) = \rho^2$ and $d\rho = B(r)dr$, the metric can be expressed as the standard metric of a unit two-dimensional sphere $\mathbb{S}^2$:

$$d\rho^2 + \rho^2\left(d\vartheta^2 + \sin^2\vartheta d\varphi^2\right). \tag{2.50}$$

Therefore, the general form of the metric on a static and spherically symmetric spacetime can be written by replacing the Riemannian metric h in Eq. (2.48) with q as

$$\begin{aligned} g &= -Adt^2 + q \\ &= -A(r)dt^2 + B(r)dr^2 + C(r)\left(d\vartheta^2 + \sin^2\vartheta d\varphi^2\right). \end{aligned} \tag{2.51}$$

Hereafter, for simplicity, we refer to a static and spherically symmetric spacetime as an SSS spacetime.

2.4.2 Application of Fermat's principle

First, we consider the application of Fermat's principle to conformally stationary spacetimes. This case is particularly interesting in relation to the standard approximation methods (quasi-Newtonian approximations) commonly used in gravitational lensing (GL) theory. The metric of a conformally stationary spacetime

can generally be written, based on Eq. (2.47), as

$$\tilde{g} = e^{2U} g,$$
$$g = -A\left(dt - \hat{\phi}\right)^2 + h,$$

where U is an arbitrary function, $\hat{\phi}$ is a 1-form independent of t, and h is a Riemannian metric.

Along a future-directed null curve, $\tilde{g} = 0$, so

$$e^{2U}\left(-A\left(dt - \hat{\phi}\right)^2 + h\right) = 0,$$

which implies

$$dt = \hat{\phi} + \sqrt{A^{-1}h}. \tag{2.52}$$

Assuming (without loss of generality) that light is emitted at $t = 0$ and considering a stationary observer, the arrival time t of the null curve is given by

$$t = \int_0^{\ell_1} \left(\hat{\phi} + \sqrt{A^{-1}}d\ell\right), \tag{2.53}$$

where we have set $h = d\ell^2$.

Under these assumptions, Fermat's principle takes the form

$$\delta \int_0^{\ell_1} \left(\hat{\phi} + \sqrt{A^{-1}}d\ell\right) = 0. \tag{2.54}$$

Next, let us consider the static case. In this scenario, $\hat{\phi} = 0$ (see the previous subsection). Furthermore, if the Riemannian metric h is conformally Euclidean, i.e., $h = \sqrt{C}\delta_E$ (where C is a function independent of t, and δ_E is the Euclidean metric), then Eq. (2.54) reduces to

$$\delta \int_0^{\ell_{E1}} n d\ell_E = 0, \tag{2.55}$$

where

$$n \equiv \sqrt{\frac{C}{A}}, \tag{2.56}$$

and ℓ_E is the Euclidean arc length. Thus, Fermat's principle reduces to its standard optics form for an isotropic medium with index of refraction n on Euclidean space. As a consequence, light propagation in a conformally static spacetime can be mimicked by a medium with an approptiately chosen index of refraction.

The Schwarzschild metric, which is used in the numerical computations in Section 3.3, is conformally Euclidean.

2.4.3 Null orbits

Thanks to spherical symmetry, we can, without loss of generality, restrict our discussion to the equatorial plane $\{\vartheta = \pi/2\}$. Hence, the metric is simplified as

$$g = -A(r)dt^2 + B(r)dr^2 + C(r)d\varphi^2. \tag{2.57}$$

We suppose that the metric components $A(r) > 0$, $B(r) > 0$, and $C(r) > 0$ are finite. This means that we focus on the outside of the horizon if exists.

Let $\gamma : I \to \mathcal{M}$ be a null geodesic parameterized by an affine parameter v, with the tangent vector $\dot{\gamma} = (d/dv)\gamma(v)$, where I is an interval. As discussed in subsection 2.4.1, a static and spherically symmetric spacetime possesses a timelike Killing vector field $\xi = \partial_t$ and a spacelike Killing vector field $= \partial_\varphi$ with closed orbits. Along the geodesic γ, the inner products of $\dot{\gamma}$ with these Killing vector fields are conserved (See Eq. (2.3) in Subsection 2.1.1). These constants of motion are defined as

$$E := -g(\dot{\gamma}, \partial_t) = A(r)\dot{t}, \tag{2.58}$$
$$L := g(\dot{\gamma}, \partial_\varphi) = C(r)\dot{\varphi}, \tag{2.59}$$

where E is the specific energy and L is the specific angular momentum of the photon.

Using the null condition

$$g(\dot{\gamma}, \dot{\gamma}) = 0, \tag{2.60}$$

we obtain

$$A(r)B(r)\dot{r}^2 = E^2 - L^2V(r), \tag{2.61}$$

where the effective potential $V(r)$ is defined as

$$V(r) := \frac{A(r)}{C(r)}. \tag{2.62}$$

The potential $V(r)$ plays the central role in the proof of a theorem that clarifies a connection among three properties of the presence of a PS, the centrifugal force reversal and infinitely many images in any SSS spacetime [26].

Differentiating Eq. (2.62) with respect to the affine parameter yields

$$[A(r)B(r)]'\dot{r}^2 + 2A(r)B(r)\ddot{r} + L^2V'(r) = 0, \tag{2.63}$$

where the prime denotes the differentiation with respect to r. From Eqs. (2.61) and (A.7), we find that a photon orbit is circular if and only if $r = r_m$ satisfies

$V(r_m) = b_m^{-2}$ and $\tilde{V}'(r_m) = 0$, where r_m denotes the radius of the circular null geodesic and the subscript m denotes the value at $r = r_m$. From $V(r_m) = b_m^{-2}$, the impact parameter for the circular null geodesic is obtained as

$$b_m = \sqrt{\frac{C_m}{A_m}}, \tag{2.64}$$

where Eq. (2.62) is used.

2.4.4 Deflection angle of light

From Eqs. (2.59) and (2.61), the orbit equation is obtained as

$$\left(\frac{dr}{d\varphi}\right)^2 = \frac{C(r)^2\left(b^{-2} - V(r)\right)}{A(r)B(r)}, \tag{2.65}$$

where

$$b := \frac{L}{E} \tag{2.66}$$

is the impact parameter of light. Without loss of generality, we assume $b > 0$ due to the spherical symmetry.

We denoted the closest approach of a light ray as r_0, which satisfies $V(r_0) = b^{-2}$. Henceforth, we use the subscript 0 when we evaluate any functions at $r = r_0$. For example, $V(r_0) = b^{-2}$ is equivalent to $V_0 = b^{-2}$, By using Eq. (2.62), we obtain

$$b = \sqrt{\frac{C_0}{A_0}}. \tag{2.67}$$

This equation tells us a relation between b and r_0.

By integrating Eq. (2.65) from a source (denoted as S) to an observer (denoted as O), we obtain the total change in the longitudinal angle,

$$I(r_0, r_S, r_O) \equiv \sum_{i=S,O} \int_{r_0}^{r_i} \sqrt{\frac{A(r)B(r)}{b(r_0)^{-2} - V(r)}} \frac{dr}{C(r)}. \tag{2.68}$$

Here, we assume that

$$\lim_{r\to\infty} A(r) = \lim_{r\to\infty} B(r) = \lim_{r\to\infty} r^{-2}C(r) = 1. \tag{2.69}$$

Then, the deflection angle of light is defined, following [5], [6], and [66], by taking the limits $r_O \to \infty$ and $r_S \to \infty$ as

$$\alpha(r_0) \equiv I_\infty(r_0) - \pi, \tag{2.70}$$

where we define $I_\infty(r_0)$ as

$$I_\infty(r_0) \equiv 2\int_{r_0}^{\infty} \sqrt{\frac{A(r)B(r)}{b(r_0)^{-2} - V(r)}} \frac{dr}{C(r)}. \tag{2.71}$$

The expression for the deflection angle given in Eq. (2.70) shall be used in the numerical computations in Section 3.3.

For the behavior of light rays around the photon sphere of a compact star, see Appendix B.

Chapter 3

Correspondence between two gravitational lens equations

This chapter is the main part of this thesis and is based on [40]. First, Section 3.1 discusses two very accurate gravitational lens equations usually used in asymptotically flat, static, and spherically symmetric spacetimes: the Virbhadra-Ellis (VE) equation and the Ohanian-Bozza (OB) equation. In particular, it is argued that the VE equation contains an unphysical branch and therefore should be improved (Subsections 3.1.2 - 3.1.6). In Section 3.2, a deflection angle transformation formula is derived to connect the improved VE equation and the OB equation. Finally, Section 3.3 numerically examines the extent to which the VE and OB equations differ when the deflection angle transformation is ignored.

3.1 Two lens equations

3.1.1 VE and OB equations

We begin with a review of two gravitational lens equations that allow for the strong deflection of light near a compact object such as a black hole. Both equations describe the mapping between the angular position of the source β on the source plane and the angular position of the image θ in terms of angular diameter distances in rigorous manners (e.g. See Figure 3.1), and are formulated based on Euclidean geometry. In the case of a static and spherically symmetric spacetime, this is allowed (see Subsection 2.4.2). D_L, D_S and D_{LS} are the angular diameter

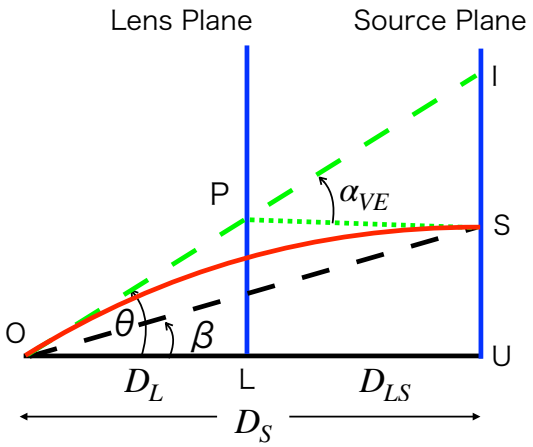

Figure 3.1: The deflection occurs at the point P on the lens plane. The deflection angle α_{VE} is assumed to be positive in this figure.

distances between the observer and the lens plane, between the observer and the source plane, and between the lens and the source plane, respectively.

A crucial difference between the two equations lies in how the deflection angles of light are defined. As shown in Figure 3.1, Virbhadra and Ellis assumed an almost aligned configuration, as is typically done in conventional lens equations with the thin lens approximation [52].

From Figure 3.1, we read off

$$\begin{aligned} UI &= D_S \tan\theta, \\ US &= D_S \tan\beta, \\ SI &= D_{LS}\left[\tan\theta + \tan(\alpha_{VE} - \theta)\right], \end{aligned}$$

where the distance D_L, D_{LS}, and $D_S = D_L + D_{LS}$ refer to the Euclidean background and α_{VE} is the deflection angle of light defined at the point P on the lens plane in Figure 3.1. The equation $UI = US + SI$ gives the VE equation

$$D_S \tan\beta = D_S \tan\theta - D_{LS}[\tan\theta + \tan(\alpha_{VE} - \theta)]. \tag{3.1}$$

To avoid an almost aligned assumption, Ohanian considered the tangent line at the source and that at the observer (See Figure 3.2) and the intersection point Q [44]. Note that the intersection point Q is generally off the lens plane. For the quadrilateral OLSQ (See Figure 3.2), we can find a relation among the four interior angles:

$$\theta + \bar{\theta} + \Delta\phi - \pi - \alpha_{OB} = 0, \tag{3.2}$$

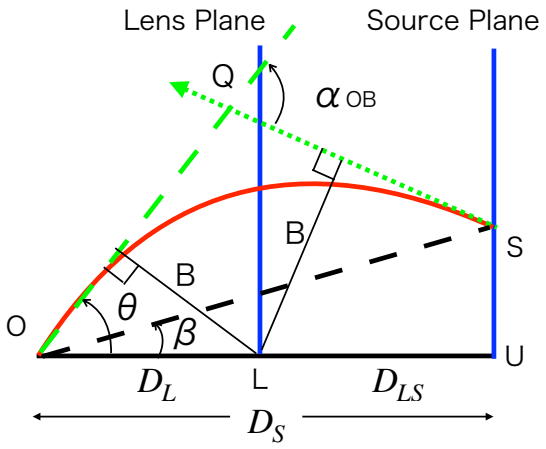

Figure 3.2: The deflection point Q in the OB equation is off the lens plane.

where $\bar{\theta} = \angle OSQ$, $\Delta\phi = \angle OLS$, and α_{OB} is the deflection angle of light defined at the intersection point Q in Figure 3.2. This is the Ohanian relation [44]. Bozza rewrote it in terms of the angular diameter distances to arrive at an improved version of an very accurate lens equation.

B in Figure 3.2 denotes the impact parameter of the light ray from S to O. We can write B in two ways:

$$B = D_L \sin\theta,$$
$$B = -\frac{D_{LS}}{\cos(\Delta\phi)} \sin\bar{\theta},$$

Eliminating B from these equations gives

$$\sin\bar{\theta} = -\frac{D_L}{D_{LS}} \cos(\Delta\phi) \sin\theta. \tag{3.3}$$

On the other hand, from Eq. (3.2) we obtain

$$\begin{aligned} \sin\bar{\theta} &= \sin(\alpha_{OB} - \theta + \pi - \Delta\phi) \\ &= \sin(\alpha_{OB} - \theta)\cos(\Delta\phi) + \cos(\alpha_{OB} - \theta)\sin(\Delta\phi). \end{aligned} \tag{3.4}$$

By substituting the above equation into Eq. (3.3) and dividing $\cos(\Delta\phi) \neq 0$ by both sides of the obtained equation, we have

$$-D_{LS}\sin(\alpha_{OB} - \theta) - D_{LS}\cos(\alpha_{OB} - \theta)\tan(\Delta\phi) = D_L \sin\theta. \tag{3.5}$$

Since we find $D_S \tan\beta = D_{LS}\tan(\pi - \Delta\phi) = -D_{LS}\tan(\Delta\phi)$ from Fig. 3.2, we therefore obtain the OB equation as

$$D_S \tan\beta = \frac{D_L \sin\theta - D_{LS}\sin(\alpha_{OB} - \theta)}{\cos(\alpha_{OB} - \theta)}. \tag{3.6}$$

By applying the Gauss-Bonnet theorem for a polygon to the gravitational lens [22], Takizawa *et.al.* derived another accurate lens equation as [60]

$$\begin{aligned}&\alpha_{TOA} - \theta - \arcsin\left(\frac{D_L}{\sqrt{(D_{LS})^2 + (D_S)^2\tan^2\beta}}\sin\theta\right)\\&+ \arctan\left(\frac{D_S}{D_{LS}}\tan\beta\right)\\&= 0,\end{aligned} \tag{3.7}$$

where α_{TOA} is defined at the intersection point Q in Figure 3.2. They also showed theat this equation is equivalent to Eq. (3.6) [60]. Therefore, $\alpha_{OB} = \alpha_{TOA}$.

3.1.2 Duality in VE equation

Using $D_S = D_L + D_{LS}$ and the tangent addition formula,

$$\tan(\theta_1 + \theta_2) = \frac{\tan\theta_1 + \tan\theta_2}{1 - \tan\theta_1\tan\theta_2},\ \forall\theta_1, \theta_2 \in \mathbb{R}$$

we can rewrite Eq. (3.1) as a quadratic in $\tan\theta$;

$$\begin{aligned}(3.1) &\iff D_S\tan\beta = D_L\tan\theta - D_{LS}\tan(\alpha_{VE} - \theta)\\&\iff D_S\tan\beta\,(1 + \tan\alpha_{VE}\tan\theta)\\&\qquad = D_L\tan\theta\,(1 + \tan\alpha_{VE}\tan\theta) - D_{LS}\,(\tan\alpha_{VE} - \tan\theta)\\&\iff D_L\tan\alpha_{VE}(\tan\theta)^2 + D_S(1 - \tan\beta\tan\alpha_{VE})\tan\theta\\&\qquad - (D_S\tan\beta + D_{LS}\tan\alpha_{VE}) = 0.\end{aligned} \tag{3.8}$$

In Figure 3.1, one might expect that a positive $\tan\theta$ would exist uniquely for a given α_{VE}. However, this is not the case. Eq. (3.1) is equivalent to Eq. (3.8), which admits two solutions for $\tan\theta$. One of these solutions corresponds to Figure 3.1, whereas the other $\tan\theta$ is unphysical because it does not describe the light ray shown in Figure 3.1.

For α_{VE} in Figure 3.1, Eq. (3.8) is formally solved for $\tan\theta$ as

$$\tan\theta = \frac{D_S(\tan\beta\tan\alpha_{VE} - 1) \pm \sqrt{\mathcal{D}}}{2D_L\tan\alpha_{VE}}, \tag{3.9}$$

where

$$\begin{aligned}\mathcal{D} \equiv&(D_S)^2(\tan\beta\tan\alpha_{VE} - 1)^2\\&+ 4D_L\tan\alpha_{VE}(D_S\tan\beta + D_{LS}\tan\alpha_{VE}).\end{aligned} \tag{3.10}$$

By straightfoward calculations, $\mathcal{D}$ can be rewritten as

$$\begin{aligned}\mathcal{D} &= \left((D_S)^2\tan^2\beta + 4D_L D_{LS}\right)(\tan\alpha_{VE})^2 \\ &\quad - 2D_S\tan\beta\,(D_{LS}-D_L)\tan\alpha_{VE} + (D_S)^2 \\ &= A\left(\tan\alpha_{VE} - \frac{B}{A}\right)^2 + \frac{4D_L D_{LS}(D_S)^2}{A\cos^2\beta},\end{aligned} \tag{3.11}$$

where $A \equiv (D_S)^2\tan^2\beta + 4D_L D_{LS}$, $B \equiv D_S(D_{LS}-D_L)\tan\beta$, and $A > 0$. Eq. (3.11) shows that $\mathcal{D} > 0$ for any α_{VE}.

The plus and minus signs in Eq. (3.9) reflect two branches in VE equation. Note that Eq. (3.9) does not mean a solution for the lens equation for which α_{VE} is not a given number but it should be treated as a function of θ. Eq. (3.9) is still an equation for θ as shown later.

3.1.3 Unphysical configuration for VE equation

In this subsection, we shall examine what is the unphysical branch in VE equation. First, we consider another configuration of the observer, lens and source system shown by Figure 3.3, where α_{VE2} denotes the deflection angle. Note that $0 < \alpha_{VE} < \pi$ and $-\pi < \alpha_{VE2} < 0$ in Figures 3.1 and 3.3, respectively. For the strong deflection of a relativistic image, $2N\pi < \alpha_{VE} < (2N+1)\pi$ in Figure 3.1 and $-(2N+1)\pi < \alpha_{VE2} < -2N\pi$ in Figure 3.3 for $N = 1, 2, \cdots$, where N is an integer which corresponds to the winding number of the light ray. We consider the deflection of light, for which $\alpha_{VE} \neq 0$ and $\alpha_{VE2} \neq 0$.

Here, let us set $\alpha_{VE2} = \alpha_{VE} - \pi$ ($\alpha_{VE2} = \alpha_{VE} - (4N+1)\pi$ for a pair of relativistic images with the winding number N), which leads to $\tan\alpha_{VE2} = \tan\alpha_{VE}$. This means that the different configuration specified by $\alpha_{VE2}(\neq \alpha_{VE})$ satisfies the same lens equation as Eq. (3.1). Therefore, Eq. (3.1) for $\tan\theta$ has two solutions, where one solution corresponds to Figure 3.1 and the other describes Figure 3.3. The angle θ for the physical configuration in Figure 3.1 is greater than θ for the unphysical configuration in Figure 3.3.

In the weak deflection of light, the image in Figure 3.1 is called the primary image on the same side of the intrinsic source position with respect to the lens [52]. Thus, $\tan\theta$ in Figure 3.1 is greater than that in Figure 3.3. Up to this point, we have focused on $\alpha_{VE} > 0$.

Next, we consider the case of $\alpha_{VE} < 0$, for which Figure 3.3 corresponds to a physical configuration, whereas Figure 3.1 is unphysical. In the weak deflection, therefore, the image in Figure 3.3 is the secondary image on the opposite side of the intrinsic source position with respect to the lens [52].

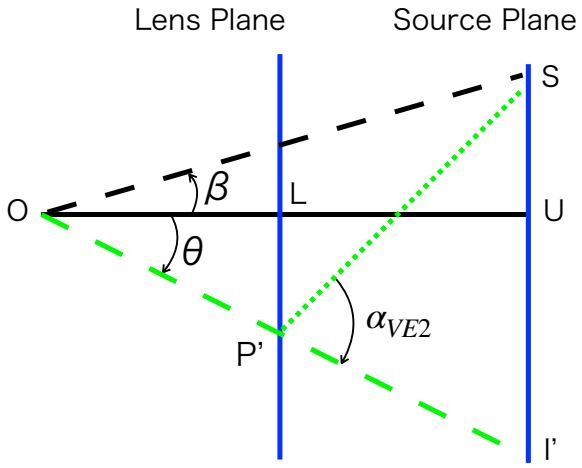

Figure 3.3: Another deflection point P' is located on the lens plane. Here, α_{VE2} is negative.

3.1.4 Duality in VE solutions

In this subsection, let us classify two branches in VE equation. For our graphical method, it is convenient to rewrite Eq. (3.1) as

$$\frac{D_L}{D_{LS}}\tan\theta - \frac{D_S}{D_{LS}}\tan\beta = \frac{\tan\alpha_{VE} - \tan\theta}{1+\tan\alpha_{VE}\tan\theta}, \tag{3.12}$$

where $D_S - D_{LS} = D_L$ is used.

Note that $\tan\theta$ satisfying Eq. (3.12) corresponds to an intersection point between a straight line given by

$$y = ax - b, \tag{3.13}$$

and a hyperbolic curve given by

$$y = \frac{c-x}{1+cx}, \tag{3.14}$$

where $x \equiv \tan\theta$, $a \equiv D_L/D_{LS} \geq 0$, $b \equiv D_S\tan\beta/D_{LS}$, and $c \equiv \tan\alpha_{VE}$.

For the remainder of this section, we assume $\tan\beta \geq 0$ without loss of generality, thanks to spherical symmetry. Thus, $b \geq 0$. On the other hand, the sign of c is arbitrary, as $-\infty < \tan\alpha_{VE} < +\infty$. Since the light ray is deflected, $c = \tan\alpha_{VE} \neq 0$.

There are four possible types of intersections:
(1) For $c > 0$, see Figure 3.4 for schematic plots of Eqs. (3.13) and (3.14). From this figure, we find $x(=\tan\theta)$ of one intersection is positive, whereas the other is

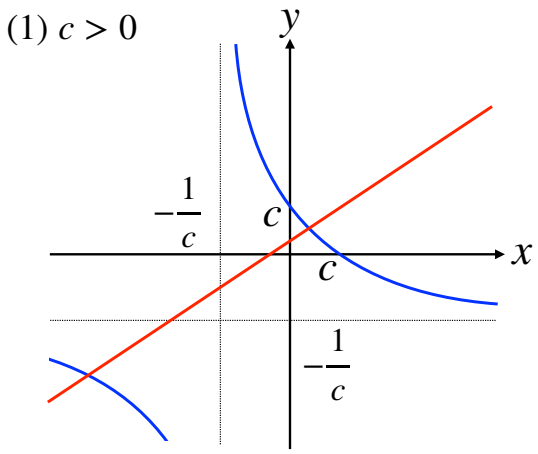

Figure 3.4: $c \equiv \tan\alpha_{VE} > 0$. There are two solutions of VE equation . The red (in color) line denotes Eq. (3.13) and the blue (in color) curves mean Eq. (3.14). They have two intersection points. One of the intersections is $x > 0$ and the other is $x < 0$.

negative. The former and latter intersections correspond to Figures 3.1 and 3.3, respectively.

(2) For $-b < c < 0$, see Figure 3.5. x for both solutions is positive. Only for this case, there are no solutions corresponding to Figure 3.3.

(3) For $-b = c < 0$, one solution for x is positive and the other is $x = 0$. However, the latter case corresponds to the lens direction $\theta = 0$. Since this direction is not observable, it can be ignored.

(4) For $c < -b$, see Figure 3.6. One solution is positive and the other is negative.

In schematic plots in Figures 3.4-3.6, $\tan\theta$ at an intersection is a real number.

Note that not all of the above cases (1)-(4) are necessarily realized. Special care is needed for case (2), as explained below.

In Figure 3.1, one might expect that a positive $\tan\theta$ exists uniquely for a given α_{VE}. However, in case (2), there are two positive solutions for $\tan\theta$. This means that while one $\tan\theta$ corresponds to Figure 3.1, the other solution is unphysical because it does not correspond to the configuration shown in Figure 3.1.

In deriving Eq. (3.1), Figure 3.1 is assumed, where $\tan\theta \geq 0$ is implicitly assumed. Therefore, for this setup, the negative values of x in cases (1) and (4) must be excluded. As a result, an unphysical branch may exist in Eq. (3.1).

Let us consider the case where $\tan\theta < 0$. This case cannot be described by Eq. (3.1) if α_{VE} is the same as for $\tan\theta \geq 0$. In this case, Figure 3.1 should be

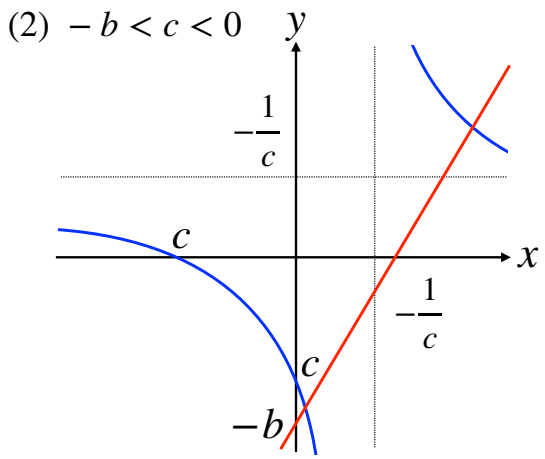

Figure 3.5: $-b < c < 0$, where $b = D_S(\tan\beta)/D_{LS}$. There are two solutions of VE equation. The red (in color) line denotes Eq. (3.13) and the blue (in color) curves mean Eq. (3.14). They have two intersection points. Both of the intersections are $x > 0$.

replaced by Figure 3.3, which leads to a different VE equation with a different deflection angle, α_{VE2}, as shown in Figure 3.3. Note that α_{VE2} is not equal to α_{VE}.

3.1.5 On the minus branch of VE equation

In this subsection, we show that there exists no solution corresponding to a lensed image in the minus branch of the VE equation:

$$\tan\theta = \frac{D_S(\tan\beta\tan\alpha_{VE} - 1) - \sqrt{\mathcal{D}}}{2D_L\tan\alpha_{VE}}, \tag{3.15}$$

in a relativistic compact object. A relativistic compact object has a photon sphere. Therefore, the closest distance r_0 of a light ray is small, i.e., $r_0 \ll D_S$.

The VE equation considers the observer and the source in asymptotic flat regions but not in the neighborhood of the lens. Hence, $D_L D_{LS}(D_S)^{-2} \ll 1$ is not allowed. The VE equation also assumes a nearly coaligned configuration, i.e., a small $\tan\beta$. Thus, it suffices to assume $|\tan\beta| < 1$.

For convenience in the following calculations, we denote

$$r \equiv \frac{D_L}{D_S} \in (0,1),$$
$$s \equiv \tan\beta,$$
$$t \equiv \frac{1}{\tan\alpha_{VE}}.$$

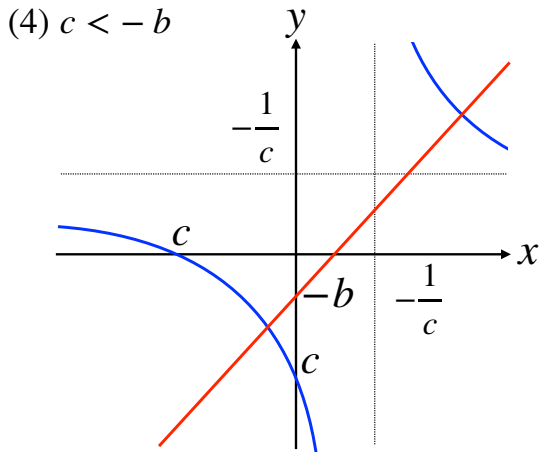

Figure 3.6: $c < -b$. There are two solutions of VE equation. The red (in color) line denotes Eq. (3.13) and the blue (in color) curves mean Eq. (3.14). They have two intersection points. One of the intersections is $x > 0$ and the other is $x < 0$.

Thanks to the spherical symmetry, we can choose $s \geq 0$ without loss of generality. Equation (3.15) can then be re-expressed as

$$\tan\theta = \frac{s - f(t)}{2r}, \tag{3.16}$$

where

$$\begin{aligned} D_{LS} &= (1-r)/D_S, \\ f(t) &\equiv t + \frac{t}{|t|}\sqrt{\tilde{\mathcal{D}}}, \\ \tilde{\mathcal{D}} &\equiv \frac{t^2}{D_S}\mathcal{D} = p - 2qt + t^2 > 0, \\ p &\equiv s^2 + 4r(1-r) > 0, \\ q &\equiv s(1-2r). \end{aligned} \tag{3.17}$$

Note that q can take both positive and negative values since $1 - 2r = (D_{LS} - D_L)/D_S$. By straightfoward calculation, we have an inequality for $|q|$:

$$\begin{aligned} p - q^2 &= s^2 + 4r(1-r) - s^2\left(1 - 4r(1-r)\right) \\ &= 4r(1-r)(1+s^2) > 0 \\ \Longrightarrow |q| &< p. \end{aligned}$$

First, we consider the case where $t > 0$. In this case, Equation (3.17) becomes

$$f(t) = t + \sqrt{p - 2qt + t^2}.$$

Its derivative with respect to t is

$$\frac{d}{dt}f(t) = \frac{\sqrt{p-2qt+t^2}+(t-q)}{\sqrt{p-2qt+t^2}} > 0.$$

This means that $f(t)$ is a monotonically increasing function for $t > 0$. Therefore, for all $t > 0$, $f(t) > \lim_{t\to 0} f(t) = \sqrt{p} > s$. We thus obtain

$$|\tan\theta| = \frac{f(t)-s}{2r} > \frac{\sqrt{p}-s}{2r}. \tag{3.18}$$

For $s < 1$,

$$\begin{aligned}\sqrt{p}-s &= \sqrt{s^2+4r(1-r)}-s \\ &> \sqrt{1+4r(1-r)}-1 \\ &= \frac{4r(1-r)}{\sqrt{1+4r(1-r)}+1} \\ &\geq \frac{4r(1-r)}{1+\sqrt{2}},\end{aligned} \tag{3.19}$$

where we used $1+\sqrt{1+4r(1-r)} \leq 1+\sqrt{2}$ for the last inequality. Using inequality (3.19) in inequality (3.18) yields

$$|\tan\theta| > \frac{1}{2r}\cdot\frac{4r(1-r)}{1+\sqrt{2}} = \frac{2}{1+\sqrt{2}}\frac{D_{LS}}{D_S}. \tag{3.20}$$

This result leads to the closest distance of a light ray

$$r_0 = D_L\,|\tan\theta| > \frac{2}{1+\sqrt{2}}\frac{D_L D_{LS}}{D_S}. \tag{3.21}$$

This result, however, contradicts $r_0 \ll D_S$ since $D_L D_{LS}(D_S)^{-2} \ll 1$ is not allowed. Therefore, for $t > 0$, the minus branch of the VE equation has no solution corresponding to a lensed image.

Next, we consider the case where $t < 0$. We then obtain

$$f(t) = t - \sqrt{p-2qt+t^2}, \tag{3.22}$$

which is a negative function for $t < 0$. Its derivative with respect to t is

$$\begin{aligned}\frac{d}{dt}f(t) &= \frac{\sqrt{p-2qt+t^2}-(t-q)}{\sqrt{p-2qt+t^2}} \\ &= \frac{\sqrt{(t-q)^2+p-q^2}-(t-q)}{\sqrt{p-2qt+t^2}} \\ &> 0,\end{aligned}$$

because $p > q^2$ was used for the last inequality. Hence, since $f(t)$ is also a monotonically increasing function for $t < 0$, $f(t) < \lim_{t\to 0} f(t) = \sqrt{p}$ for all $t < 0$. We thus find

$$\begin{aligned} |\tan\theta| &= \frac{|s - f(t)|}{2r} \\ &= \frac{s + |f(t)|}{2r} \\ &> \frac{\sqrt{p} + s}{2r}. \end{aligned} \tag{3.23}$$

By Using $\sqrt{p} + s \geq 2\sqrt{r(1-r)}$ in Eq. (3.23), we can get

$$|\tan\theta| > \frac{2\sqrt{r(1-r)}}{2r} = \sqrt{\frac{D_{LS}}{D_L}}, \tag{3.24}$$

which leads to the closest distance of a light ray

$$r_0 = D_L\,|\tan\theta| > \sqrt{D_L D_{LS}}. \tag{3.25}$$

However, this inequality contradicts $r_0 \ll D_S$ since $D_L D_{LS}(D_S)^{-2} \ll 1$ is not allowed. Thus, the minus branch of the VE equation also has no solution corresponding to a lensed image for $t < 0$.

In either case, there exists no solution corresponding to a lensed image in the minus branch of the VE equation. Therefore, Eq. (3.15) represents the unphysical branch.

3.1.6 Improved VE equation

In the previous subsection, it was shown that the minus branch of the VE equation is unphysical. Therefore, only the plus branch of the VE equation, obtained by removing the minus branch, contains the solutions corresponding to lensed images. Hence, we call the plus branch of the VE equation

$$\tan\theta = \frac{D_S(\tan\beta\tan\alpha_{VE} - 1) + \sqrt{\mathcal{D}}}{2D_L\tan\alpha_{VE}}. \tag{3.26}$$

the *improved VE equation*.

Indeed, it can be shown that the improved VE equation reduces to the lens equation (1.1) in the weak gravitational field under the small-angle approximation

(i.e., $|\beta| \ll 1$, $|\theta| \ll 1$ and $|\alpha_{VE}(\theta)| \ll 1$). Expanding $\sqrt{\mathcal{D}}$, we obtain

$$\begin{aligned}\sqrt{\mathcal{D}} &= D_S\sqrt{(\tan\beta\tan\alpha_{VE}-1)^2+4\frac{D_L}{D_S}\tan\alpha_{VE}\left(\tan\beta+\frac{D_{LS}}{D_S}\tan\alpha_{VE}\right)} \\ &= D_S\sqrt{1-2\beta\alpha_{VE}+4\frac{D_L}{D_{LS}}\left(\beta\alpha+\frac{D_{LS}}{D_S}\alpha_{VE}^2\right)+O(\alpha_{VE}^3,\beta^3)} \\ &= D_S\left[1-\beta\left(1-2\frac{D_L}{D_S}\right)\alpha_{VE}+2\frac{D_LD_{LS}}{(D_S)^2}\alpha_{VE}^2\right]+O(\alpha_{VE}^3,\beta^3). \qquad (3.27)\end{aligned}$$

Substituting Eq.(3.27) into Eq. (3.26) yields

$$\begin{aligned}\theta+O(\theta^3) &= \frac{D_S}{2D_L\alpha_{VE}}\left[\beta\alpha_{VE}-1+1-\beta\left(1-2\frac{D_L}{D_S}\right)\alpha_{VE}+2\frac{D_LD_{LS}}{(D_S)^2}\alpha_{VE}^2\right] \\ &\quad +O(\alpha_{VE}^3,\beta^3) \\ &= \beta+\frac{D_{LS}}{D_S}\alpha_{VE}+O(\alpha_{VE}^2,\beta^2), \\ \therefore\ \beta &= \theta-\frac{D_{LS}}{D_S}\alpha_{VE}(\theta)+O(\theta^3,\alpha_{VE}^2,\beta^2), \qquad (3.28)\end{aligned}$$

which is consistent with the lens equation (1.1) in the weak gravitational field. We thus find that the imploved VE equation contains the ordinary solutions.

On the other hand, the minus branch of the VE equation cannot take the small-angle approximation since the divergent term appears under this approximation:

$$\begin{aligned}\theta+O(\theta^3) &= \frac{D_S}{2D_L\alpha_{VE}}\left[\beta\alpha_{VE}-1-\left(1-\beta\left(1-2\frac{D_L}{D_S}\right)\alpha_{VE}+2\frac{D_LD_{LS}}{(D_S)^2}\alpha_{VE}^2\right)\right] \\ &\quad +O(\alpha_{VE}^3,\beta^3) \\ &= -\frac{D_S}{D_{LS}}\frac{1}{\alpha_{VE}}+\frac{D_S}{D_{LS}}\beta-\beta-\frac{D_{LS}}{D_S}\alpha_{VE}+O(\alpha_{VE}^2,\beta^2).\end{aligned}$$

3.2 Correspondence between VE and OB equations

For the same configuration of the lens, observer and source with given β and θ, the improved VE and OB equations should be equal. For Eq. (3.26) to equal

to Eq. (3.6), we have

$$\frac{D_{LS}\sin\alpha_{OB}+D_S\tan\beta\cos\alpha_{OB}}{D_L+D_{LS}\cos\alpha_{OB}-D_S\tan\beta\sin\alpha_{OB}}=\frac{D_S(\tan\beta\tan\alpha_{VE}-1)+\sqrt{\mathcal{D}}}{2D_L\tan\alpha_{VE}}$$
$$\iff 2D_L\tan\alpha_{VE}\frac{E(\alpha_{OB})}{F(\alpha_{OB})}-D_S(\tan\beta\tan\alpha_{VE}-1)=\sqrt{\mathcal{D}}. \tag{3.29}$$

where we define functions E and F of α_{OB} as

$$E(\alpha_{OB})\equiv D_{LS}\sin\alpha_{OB}+D_S\tan\beta\cos\alpha_{OB}, \tag{3.30}$$
$$F(\alpha_{OB})\equiv D_L+D_{LS}\cos\alpha_{OB}-D_S\tan\beta\sin\alpha_{OB}. \tag{3.31}$$

By squaring both sides of Eq. (3.29) and dividing $\tan\alpha_{VE}(\neq 0)$, we can get

$$D_L(\tan\alpha_{VE})^2\frac{E^2}{F^2}-D_S\tan\alpha_{VE}(\tan\beta\tan\alpha_{VE}-1)\frac{E}{F}$$
$$=\tan\alpha_{VE}(D_S\tan\beta+D_{LS}\tan\alpha_{VE})$$
$$\implies\left[D_L\frac{E^2}{F^2}-D_S\tan\beta\frac{E}{F}-D_{LS}\right]\tan\alpha_{VE}=D_S\left(-\frac{E}{F}+\tan\beta\right).$$

Hence, the relationship between α_{VE} and α_{OB} must be

$$\tan\alpha_{VE}=\frac{D_SF(E-F\tan\beta)}{D_{LS}F^2+D_SEF\tan\beta-D_LE^2}, \tag{3.32}$$

Figure 3.7 shows a relation between α_{VE} and α_{OB} in Eq. (3.32).

It is worth mentioning that the OB equation, Eq. (3.6), can be simply rewritten in terms of E and F as:

$$\tan\theta=\frac{E}{F}. \tag{3.33}$$

3.3 Numerical differences by ignoring the deflection angle transformation

Let us consider two cases: $D_L \ll D_{LS}$ and $D_L \gg D_{LS}$. For $D_L \ll D_{LS}$, we expand Eq. (3.32) in terms of D_L/D_{LS} as

$$\tan\alpha_{VE}-\tan\alpha_{OB}=O\left(\frac{D_L}{D_{LS}}\right). \tag{3.34}$$

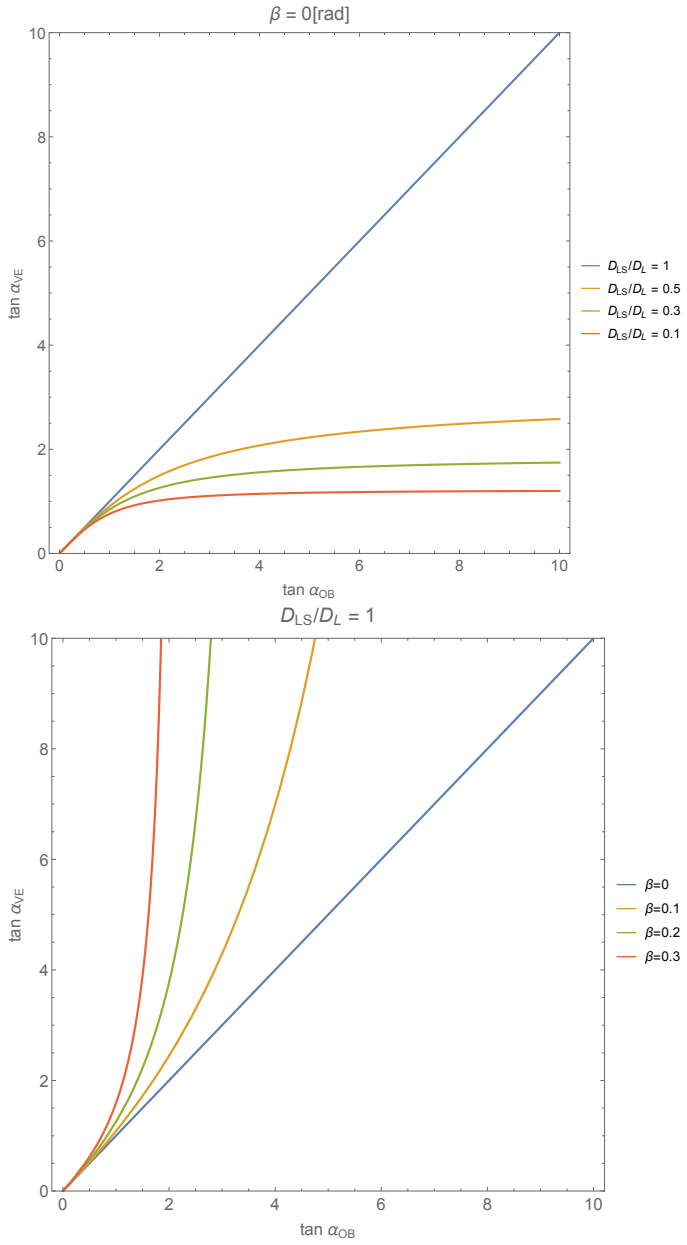

Figure 3.7: $\tan\alpha_{VE}$ vs $\tan\alpha_{OB}$. Top: $\beta = 0$, and $D_{LS}/D_L = 1$ (blue), 0.5 (orange), 0.3 (green) and 0.1 (red). Bottom: The equidistance case. $\beta = 0$ (blue), 0.1 (orange), 0.2 (green) and 0.3 (red).

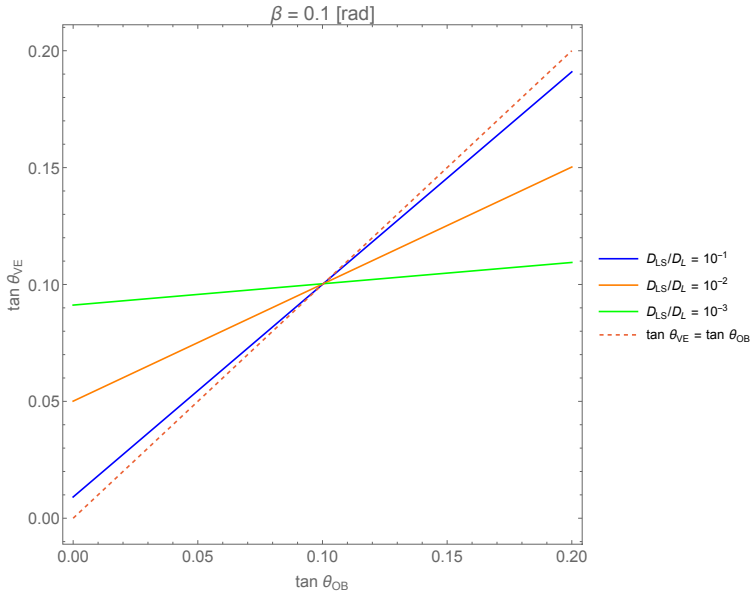

Figure 3.8: $\tan\theta_{VE}$ and $\tan\theta_{OB}$. Here, the transformation of α_{VE} is ignored when we solve the improved VE equation. The dashed line corresponds to $\tan\theta_{VE} = \tan\theta_{OB}$ as a reference. $D_{LS}/D_L = 10^{-1}$ (blue), 10^{-2} (red), and 10^{-3} (green), where $\beta = 0.1$ is chosen.

Thus, α_{VE} is very close to α_{OB}. This implies that substituting α_{OB} for α_{VE} in Eq. (3.1) provides a good approximation, even if the transformation is neglected.

On the other hand, for $D_L \gg D_{LS}$, we expand Eq. (3.32) in terms of D_{LS}/D_L as

$$\tan\alpha_{VE} - \tan\alpha_{OB} = -\frac{1}{\tan\beta\cos\alpha_{OB}} + O\left(\frac{D_{LS}}{D_L}\right). \tag{3.35}$$

This implies that the difference between α_{VE} and α_{OB} can be significantly large in the limit as $D_{LS}/D_L \to 0$, especially for nearly coaligned configurations $\beta \sim 0$. This case, where $D_L \gg D_{LS}$ and $\beta \sim 0$, corresponds to to the observation of photons from centers of galaxies, notably n the vicinity of a photon sphere of the massive black hole candidate in Sgr A*.

How large are numerical differences when we ignore the transformation between the two deflection angles? To investigate this, we assume α_{VE} and α_{OB} are equal. First, we focus on the case where $|\tan\alpha_{VE}| \ll 1$ and $|\tan\alpha_{OB}| \ll 1$. From Eqs. (3.1) and (3.6), then, we obtain

$$\frac{\tan\theta_{VE} - \tan\beta}{\dfrac{D_{LS}}{D_S}(1+\tan^2\beta)} = \frac{\tan\theta_{OB} - \tan\beta}{\dfrac{D_{LS}}{D_S} + \tan^2\beta} + O(\tan^2\alpha_{VE}, \tan^2\alpha_{OB}), \tag{3.36}$$

where θ_{VE} and θ_{OB} denote a solution to Eqs. (3.1) and (3.6), respectively. Below, we ignore the second order in $\tan\alpha_{OB}$.

For $\tan\theta_{VE}$ to equal $\tan\theta_{OB}$, the two denominators in Eq. (3.36) must be the same. However, it is not the case. See Figure 3.8 for numerical plots of Eq. (3.36).

The two denominators are very close to each other, if and only if $|\beta| \ll 1$ and $D_L \ll D_{LS}$. This condition implies that the observer, lens and source are nearly coaligned and the observer is close to the lens. This condition is not satisfied for most of astronomical situations.

The exceptional case is the gravitational lens by the Sun. In many astronomical cases ($\beta \neq 0$ and $D_L \gg D_{LS}$), conversely speaking, the ignorance of the transformation between the deflection angles would result in a significant difference between $\tan\theta_{VE}$ and $\tan\theta_{OB}$.

In the numerical calculation, we model the Sgr A^* as a Schwarzschild black hole lens. The expression for the deflection angle given in Eq. (2.70) in Subsection 2.4.4 is used.

See Figure 3.9 for the result of numerical calculations of the difference when the transformation is ignored. The numerical plots in this figure are consistent with an expression as

$$\tan\alpha_{VE} - \tan\alpha_{OB} = \frac{D_L}{D_{LS}} \sin^2\beta \tan\alpha_{OB} + O\left(\tan^2\alpha_{OB}\right), \tag{3.37}$$

which can be derived from Eq. (3.32) in the approximation as $|\tan\alpha_{OB}| \ll 1$. Eq. (3.37) is consistent with also Figure 3.7 in the domain of small $\tan\alpha_{OB}$.

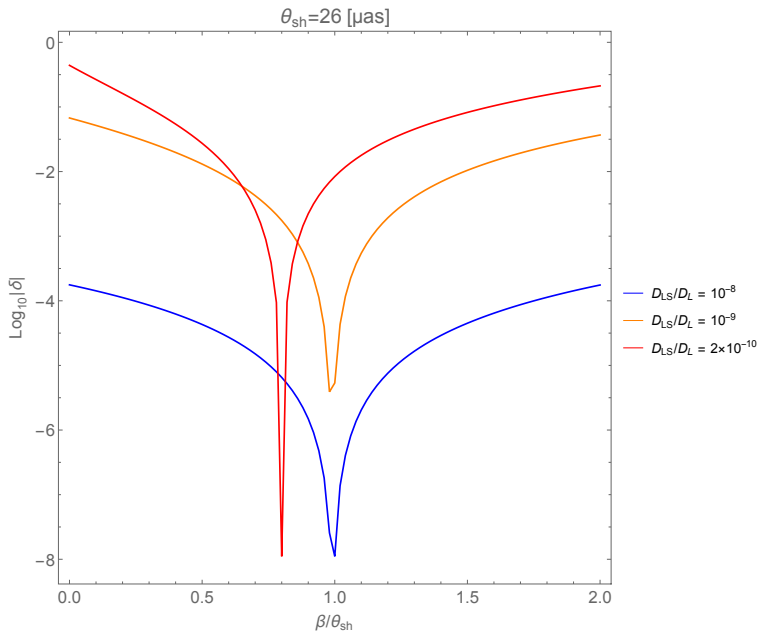

Figure 3.9: Numerical differences by ignoring the transformation between α_{VE} and α_{OB} when the improved VE equation is solved. The parameters correspond to the Sgr A* [24] in the approximation of the Schwarzschild lens, where the angular radius of the black hole shadow [49] is about 26 microarcsec., $D_L = 8$ kpc, and $D_{LS}/D_L = 1.2 \times 10^{-10}$ [3]. Here, $\delta \equiv |\theta_{VE}/\theta_{OB} - 1|$ is the relative difference due to neglecting the transformation.

Chapter 4

Summary

To explore gravitational lensing in the strong gravitational field, this thesis investigated the relationship between two very accurate gravitational lens equations: the Virbhadra-Ellis (VE) equation and the Ohanian-Bozza (OB) equation. The VE equation, proposed in [66], is applicable only when the angular source position β is sufficiently small, and the angular diameter distances between the observer and the lens, D_L, and between the lens and the source plane, D_{LS}, are nearly equal. In contrast, the OB equation remains valid for arbitrary values of β and does not require the assumption that D_L and D_{LS} are approximately equal.

One of the main results of this thesis is that the VE equation includes an unphysical branch, and by excluding this branch, the VE equation is improved. It is found that the VE equation (3.1) becomes a quadratic equation in $\tan\theta$ when the addition formula for tangents is applied. On the other hand, the OB equation is transformed into a linear equation in $\tan\theta$ by the same way. This indicates that the VE equation contains solutions that do not correspond to the lens diagram. By factorizing the VE equation, Eq. (3.9) is obtained. In Eq. (3.9), the plus and minus signs reflect the duality of the VE equation. We denoted the branch with the plus sign as the plus branch and the one with the minus sign as the minus branch. We proved that the minus branch does not contain any physical solutions corresponding to lensed images. Thus, the minus branch is unphysical, and the improved VE equation is defined as the plus branch of the VE equation. In fact, it was shown that the plus branch of the VE equation reduces to the lens equation in the weak-field limit under the small-angle approximation.

Another main point is the derivation of a transformation formula between de-

flection angles defined differently for the improved VE equation and the OB equation. This result implies that the VE equation, which is previously applicable only for a small angular source position β, can be used even for large β. In addition, we model Sgr A^* as a Schwarzschild black hole lens to perform numerical computations. Numerical calculations further indicate that the proposed transformation formula for the deflection angle should be used, particularly when D_L/D_{LS} is sufficiently small.

As future work, it would be interesting to extends to stationary and axisymmetric spacetimes along this study.

Recently, the VE equation has been used for detailed discussions of image distortions of Schwarzschild lensing [67, 68]. These results imply an existence of gravitational lens invariants in the strong gravity region. Since the VE equation is improved in this study, the results in Ref. [67, 68] are expected to be different. Therefore, it would also be interesting to calculate invariants that are independent of parameters of the lens object, such as mass or angular momentum.

Finally it should be emphasized that the study of gravitational lensing in the strong gravity region is an important direction to explore the space time structure, and test the theory of gravity. In particular, it is important to investigate how the elegant results obtained in weak-field gravitational lensing (for example, see [52], [47], and [50]) can be extended. Such extensions would lead to a deeper understanding of the approximations used in the weak field thin screen approach to lensing as well as shedding light on the meaning of genericity and stability in a spacetime context.

Appendix A

Photon Sphere

In 2019 and 2022, the Event Horizon Telescope (EHT) team has succeeded in taking direct images of the immediate vicinity of the central black hole candidate of M87 galaxy and our galaxy [2, 3]. These observations have increased our renewed interest in the strong deflection of light in the strong gravitational field. In addition, the project of the next generation Event Horizon Telescope (ngEHT) is increasing the importance of the lens by strong gravity [4].

Where is the strong gravity region in a spacetime? In a static and spherically symmetric (SSS) spacetime, one of the indicators is a photon sphere (PS), which is a set of circular null geodesics, since the deflection angle of a light becomes unboundedly large if the photon sphere is unstable. More specifically, Hasse and Perlick (2002) [26] provided a theorem that establishes a connection among three properties: (1) the presence of a PS in unstable cases, marginally unstable cases, and stable cases, (2) the reversal of centrifugal force, and (3) the existence of infinitely many images in any SSS spacetime.

How should we define the strong gravity region in a spacetime with less symmetry? Although the answer has not been found yet, study is progressing through approaches that extend the photon sphere in a SSS spacetime to more generalized concepts. One such concept is the photon surface [11]. Recently, several authors have proposed generalized conceptions of the PS or the photon surface and have discussed their geometrical properties [8, 9, 25, 31, 33–37, 42, 53–55, 71–74].

In this appendix, we introduce the concept of a PS and classify the stability of PSs.

A.1 Null geodesic equations

We begin with a brief review of the null geodesic equations in a static, spherically symmetric (SSS) spacetime (see also Section 2.4).

Let us consider a SSS spacetime, for which the metric is given by

$$ds^2 = -A(r)dt^2 + B(r)dr^2 + C(r)(d\theta^2 + \sin^2\theta d\phi^2). \tag{A.1}$$

We suppose that the metric components $A(r) > 0$, $B(r) > 0$, and $C(r) > 0$ are finite. This means that we focus on the outside of the horizon if exists. Also, we do not assume the asymptotic flatness of the spacetime in this chapter. Indeed, we will consider an asymptotically non-flat case later. Without loss of generality, we can consider a photon orbit on the equatorial plane $\theta = \pi/2$ thaks to the spherical symmetry of the spacetime. On the equatorial plane in the SSS spacetime, a null geodesic has two constants of motion; One is the specific energy $E \equiv A(r)\dot{t}$ and the other is the specific angular momentum $L \equiv C(r)\dot{\phi}$, where the overdot denotes the derivative with respect to the affine parameter s along the null geodesic.

By using the two constants E and L, the impact parameter of light is defined as $b = L/E$. Without loss of generality, we assume $b > 0$.

The null condition $ds^2 = 0$ can be rewritten as

$$A(r)B(r)\dot{r}^2 + L^2\tilde{V}(r) - E^2 = 0. \tag{A.2}$$

where $\tilde{V}(r)$ is the effective potential defined by [26]

$$\tilde{V}(r) \equiv \frac{A(r)}{C(r)}, \tag{A.3}$$

This form of the effective potential is conformally invariant. This simplifies the analysis of the photon sphere and its linear perturbation with respect to the radial direction, because $\tilde{V}(r)$ depends only on the local coordinate r.

For the later convenience, we write down the first and second derivatives of $\tilde{V}(r)$,

$$\tilde{V}^{'}(r) = -\frac{A(r)D(r)}{C(r)}, \tag{A.4}$$

$$\tilde{V}^{''}(r) = -\frac{A(r)}{C(r)}\left[D^{'}(r) - D(r)^2\right], \tag{A.5}$$

where the prime denotes the differentiation with respect to r, and the functions D is defined as

$$D(r) := \frac{C'(r)}{C(r)} - \frac{A'(r)}{A(r)}. \tag{A.6}$$

A.2 Photon sphere

Differentiating Eq. (A.2) with respect to the affine parameter yields

$$[A(r)B(r)]^{'}\dot{r}^2 + 2A(r)B(r)\ddot{r} + L^2\tilde{V}^{'}(r) = 0. \tag{A.7}$$

From Eqs. (A.2) and (A.7), we find that a photon orbit is circular if and only if $r = r_m$ satisfies $\tilde{V}(r_m) = b_m^{-2}$ and $\tilde{V}^{'}(r_m) = 0$, where r_m denotes the radius of the circular photon orbit and the subscript m denotes the value at $r = r_m$. A set of circular photon orbits is called *photon sphere* in a SSS spacetime. From $\tilde{V}(r_m) = b_m^{-2}$, the impact parameter for the photon sphere (PS) is obtained as

$$b_m = \sqrt{\frac{C_m}{A_m}}, \tag{A.8}$$

where Eq. (A.3) is used.

A.3 Classification of PS stability

Let δr be a small displacement around the orbit on the PS. Expanding Eq, (A.7) up to the first order in δr yields

$$\begin{aligned}\frac{d^2}{d\lambda^2}(\delta r) &= -\frac{L^2\tilde{V}^{''}(r_m)}{2A_mB_m}\delta r \\ &= \frac{L^2D_m^{'}}{2B_mC_m}\delta r,\end{aligned} \tag{A.9}$$

where Eq. (A.5) and $D(r_m) = 0$ from $\tilde{V}^{'}(r_m) = 0$ are used.

The sign of $D_m^{'}$ determines the linear stability of the perturbed orbit, because $A(r) > 0$, $B(r) > 0$, $C(r) > 0$ and $L \neq 0$. A PS is stable if $D_m^{'} < 0$, whereas it is unstable for $D_m^{'} > 0$.

From Eq. (A.6), we obtain

$$D^{'}(r) = \frac{C''(r)}{C(r)} - \frac{A''(r)}{A(r)} - D(r)\left(\frac{C'(r)}{C(r)} + \frac{A'(r)}{A(r)}\right). \tag{A.10}$$

Since $D_m = 0$ on the PS, this is reduced to

$$D'_m = \frac{C''_m}{C_m} - \frac{A''_m}{A_m}. \tag{A.11}$$

Bozza and Tsukamoto assumed that $D'_m > 0$, that is, a PS is unstable [5, 61]. Henceforth, we focus on a stable case $D'_m < 0$. Such an unusual case is realized in a class of Weyl gravity model as shown in Section B.3 of appensix B.

Appendix B

Deflection of light around a stable photon sphere of a compact object

---

In this appendix, we discuss a behavior of light rays around a stable photon sphere of a compact object. This appendix is based on [39].

We demonstrate that the location of a stable photon sphere (PS) in a compact object is not always an edge such as the inner boundary of a black hole shadow, whereas the location of an unstable PS is known to be the shadow edge notably in the Schwarzschild black hole. If a static spherically symmetric (SSS) spacetime has the stable outermost PS, the spacetime cannot be asymptotically flat. A nondivergent deflection is caused for a photon traveling around a stable PS, though a logarithmic divergent behavior is known to appear in most of SSS compact objects with an unstable photon sphere. The reason for the nondivergence is that the closest approach of a photon is prohibited in the immediate vicinity of the stable PS when the photon is emitted from a source (or reaches a receiver) distant from a lens object. The finite gap size depends on the receiver and source distances from the lens as well as the lens parameters. The mild deflection angle of light can be approximated by an arcsine function. A class of SSS solutions in Weyl gravity exemplify the nondivergent deflection near the stable outer PS.

B.1 Deflection of light

B.1.1 Orbit equation

In order to derive the orbit equation for the null geodesic, we rewrite the equation (A.2) as

$$\dot{r}^2 + V(r) = 0, \tag{B.1}$$

where $V(r)$ is defined as

$$V(r) \equiv -\frac{L^2 F(r)}{B(r)C(r)}. \tag{B.2}$$

Here,

$$F(r) \equiv \frac{C(r)}{A(r)b^2} - 1. \tag{B.3}$$

We denoted the closest approach of a light ray as r_0, which satisfies $V(r_0) = 0$. Henceforth, we use the subscript 0 when we evaluate any functions at $r = r_0$. For example, $V(r_0) = 0$ is equivalent to $F_0 = 0$, where $F_0 \equiv F(r_0)$. By using $F_0 = 0$ and Eq. (B.3), we obtain

$$b = \sqrt{\frac{C_0}{A_0}}. \tag{B.4}$$

This equation tells us a relation between b and r_0.

B.1.2 Total angle integral

From Eq. (B.1), we obtain

$$\frac{dr}{d\phi} = \pm\sqrt{\frac{C(r)F(r)}{B(r)}}. \tag{B.5}$$

By integrating this from a source (denoted as S) to a receiver (denoted as R), we obtain the total change in the longitudinal angle,

$$I_F(r_S, r_R, r_0) \equiv \sum_{i=S,R} \int_{r_0}^{r_i} \frac{dr}{\sqrt{\frac{C(r)F(r)}{B(r)}}}. \tag{B.6}$$

Note that a conventional method discusses the total integral I for the asymptotic receiver and source ($r_R \to \infty$ and $r_S \to \infty$) e.g. [5, 16, 61], for which $I - \pi$ gives the deflection angle of light. On the other hand, we consider finite distance between the receiver and source. In order to clarify this difference, we use I_F in stead of I. In general, $I_F - \pi$ is always not the deflection angle but I_F is the dominant component of the deflection angle near a PS. This issue is beyond the scope

of this thesis. See e.g. References [29,30,45,46] on how to define geometrically the deflection angle for the finite-distance receiver and source.

Following Bozza and Tsukamoto [5,61], we introduce a variable as

$$z \equiv 1 - \frac{r_0}{r}, \tag{B.7}$$

so that we can rewrite Eq. (B.6) as

$$I_F(z_S, z_R, r_0) = \sum_{i=S,R} \int_0^{z_i} f(z, r_0) dz, \tag{B.8}$$

where we define $z_i \equiv 1 - r_0/r_i$ $(i = R, S)$,

$$H(z, r_0) \equiv \frac{CF}{B}(1-z)^4, \tag{B.9}$$

and

$$f(z, r_0) \equiv \frac{r_0}{\sqrt{H(z, r_0)}}. \tag{B.10}$$

In the next subsection, we shall examine the integrand in Eq. (B.8).

B.1.3 Analysis in the vicinity of PS

By noting $F_0 = 0$, the function H is expanded around $r = r_0$ $(z = 0)$ as

$$H(z, r_0) = \sum_{n=1}^{\infty} c_n(r_0) z^n, \tag{B.11}$$

where

$$c_1(r_0) = \frac{C_0 D_0 r_0}{B_0}, \tag{B.12}$$

$$c_2(r_0) = \frac{C_0}{B_0}\left[D_0 r_0 \left(\frac{C_0'}{C_0} - \frac{B_0'}{B_0} - 3\right) + \frac{r_0^2}{2}(D_0^2 + D_0')\right], \tag{B.13}$$

$$\begin{aligned} c_3(r_0) = \frac{C_0}{B_0}\Bigg[&D_0 r_0 \left(\frac{3B_0' r_0}{B_0} - \frac{3C_0' r_0}{C_0} - \frac{B_0' C_0' r_0^2}{B_0 C_0} - 3\right) \\ &+ \frac{r_0^2}{2}(D_0^2 + D_0')\left(\frac{C_0' r_0}{C_0} - \frac{B_0' r_0}{B_0} - 2\right) \\ &+ \frac{r_0^3}{6}\left(D_0^3 + 3D_0' D_0 + D_0''\right)\Bigg]. \end{aligned} \tag{B.14}$$

When $r_0 \approx r_m$, Eqs. (B.12) - (B.14) become

$$c_1(r_m) = 0, \tag{B.15}$$

$$c_2(r_m) = \frac{r_m^2 C_m D'_m}{2B_m}, \tag{B.16}$$

$$c_3(r_m) = \frac{r_m^2 C_m}{2B_m}\left[D'_m\left(\frac{C'_m r_m}{C_m} - \frac{B'_m r_m}{B_m} - 2\right) + \frac{r_m D''_m}{3}\right]. \tag{B.17}$$

From Eqs. (B.15) - (B.17), we obtain

$$H(z, r_m) = c_2(r_m)z^2 + O(z^3). \tag{B.18}$$

If the PS is unstable (stable), namely $D_m^{'} > 0$ ($D_m^{'} < 0$), then, $c_2(r_m) > 0$ (< 0). As pointed by Tsukamoto [61], the angle integral I_F by Eq. (B.6) is divergent logarithmically. On the other hand, the stable PS case ($c_2(r_m) < 0$) is investigated below in detail.

Before closing this section, we mention a relation of the stable outermost PS (SOPS) and asymptotic structure of the spacetime.

Propsition

If a SSS spacetime has the SOPS, the spacetime is asymptotically non-flat, for which $\tilde{V}^{'}(r) = [A(r)/C(r)]^{'}$ is positive everywhere outside the SOPS.

Proof

Let r_{SOPS} be the radius of the SOPS. At the location of the SOPS, $\tilde{V}^{'}(r_{SOPS}) = 0$ and $\tilde{V}^{''}(r_{SOPS}) > 0$. From the definition of the SOPS, there exist no PSs outside of the SOPS. Therefore, $\tilde{V}^{''}(r) > 0$ for $r > r_{SOPS}$. This means that $\tilde{V}^{'}(r)$ is an monotonic increasing function of r for $r > r_{SOPS}$. Hence, $\tilde{V}^{'}(r) > 0$ for $r > r_{SOPS}$.

Here, we further assume that the spacetime is asymptotically flat. Then, we can adapt a coordinate system in which Eq. (A.1) approaches the Minkowski metric in the polar coordinates asymptotically as $r \to \infty$, that is, $A(r) \to 1 + O(1/r)$ and $C(r) \to r^2 + O(r)$, which lead to $A^{'}(r) \to O(1/r^2)$ and $C^{'}(r) \to 2r + O(r^0)$. Thereby,

$$\begin{aligned}\tilde{V}^{'}(r) &= \left(\frac{A(r)}{C(r)}\right)^{'} \\ &= -\frac{2}{r^3} + O\left(\frac{1}{r^4}\right) \\ &\to 0,\end{aligned} \tag{B.19}$$

as $r \to \infty$. From this, we find that $\tilde{V}^{'}(r)$ has an extremum between r_{SOPS} and $r = \infty$, because of its continuity. This contradicts with that $\tilde{V}^{'}(r)$ is amonotonic

increasing function for $r > r_{SOPS}$. Therefore, the spacetime is not asymptotically flat. A proof of the proposition is finished.

According to Reference [25], if stationary, an axisymmetric, and asymptotically flat spacetime possesses light rings (LRs), the outermost LR is unstable. This implies that if a SSS spacetime with PSs is asymptotically flat, the outermost PS is also unstable. The contrapositive of this statement suggests that if the outermost PS in an SSS spacetime with PSs is stable, then the spacetime is not asymptotically flat. This provides partial support for the above proposition but does not address the positivity of $\tilde{V}'(r)$ for $r > r_{SOPS}$.

On the other hand, asymptotic flatness is allowed if the outermost PS (OPS) is unstable, with $\tilde{V}''(r_{OPS}) < 0$. In the remainder of this chapter, we consider cases where the receiver and source are located outside a stable outer PS. However, it is not specified below whether this PS is the outermost one.

Before concluding this section, let us briefly discuss the stability of spacetimes that admit a stable PS. Horizonless ultracompact objects with a stable PS may cause instabilities due to perturbations that decay slowly (at most logarithmically), eventually leading to the formation of a trapped surface [1, 7, 13, 32]. Therefore, in Section B.3, we consider a black hole model with a stable PS in Weyl gravity. Additionally, the above proposition may suggest another possibility that is compatible with the instability arguments in References [1, 7, 13, 32]. One such possibility is a compact object without a black hole horizon but with a stable PS and a cosmological horizon, which is consistent with asymptotic non-flatness. The issue of its stability is beyond the scope of this thesis.

B.2 Mild deflection near the stable outer PS

B.2.1 Stability classification of the outer PS

In the vicinity of the closest approach $z \sim 0$, higher order terms of $H(z, r_m)$ in Eq. (B.11) are negligible compared with z and z^2 terms. Hence, the dominant part of $f(z, r_0)$ for $r_0 \sim r_m$ is given by

$$f_D(z, r_0) \equiv \frac{r_0}{\sqrt{h(z)}}, \tag{B.20}$$

where $h(z)$ is defined as

$$h(z) = c_1(r_0)z + c_2(r_0)z^2. \tag{B.21}$$

The dominant part of the total angle integral, $f_D(z, r_0)$, is defined as

$$I_{FD}(z_R, z_S, r_0) \equiv \sum_{i=S,R} \int_0^{z_i} f_D(z, r_0) dz. \tag{B.22}$$

Before proceeding with the calculations of the angle integral, we first investigate a photon orbit in the stable PS case. If $c_1(r_0) < 0$, $h(z)$ is always negative for $z > 0$. This is in contradiction with the nonnegativity of $h(z)$. Hence, the case of $c_1(r_0) < 0$ is discarded. If $c_1(r_0) = 0$, then, $h(z) = c_2(r_0)z^2$. The nonnegativity of $h(z)$ together with $c_2(r_0) < 0$ admits only $z = 0$. This orbit is circular. We do not discuss this special case any more. For the last case $c_1(r_0) > 0$, the nonnegativity of $h(z)$ provides a nontrivial situation; the allowed region for z is

$$0 \leq z \leq -\frac{c_1(r_0)}{c_2(r_0)}. \tag{B.23}$$

This means that only bound orbits are allowed, whereas the scattering orbits are prohibited. Note that $h(z) = 0$ does not make the integral in Eq. (B.22) divergent. Indeed, $h(z) \sim c_1(r_0)z$ near a point $z = 0$ and $h(z) \sim -c_1(r_0)[z + c_1(r_0)/c_2(r_0)]$ near a point $z \sim -c_1(r_0)/c_2(r_0)$. At the two points, therefore, the integral of $h(z)$ is not divergent as $\sim \int z^{-1/2}dz \sim 2\sqrt{z}$. The two points $z = 0$ and $z \sim -c_1(r_0)/c_2(r_0)$ are the periastron and apastron, respectively.

B.2.2 Angle integral for the stable outer PS

From this point forward, we focus on the case of $c_1(r_0) > 0$, for which the receiver and source positions satisfy

$$0 < z_i \leq -\frac{c_1(r_0)}{c_2(r_0)}. \tag{B.24}$$

Eq. (B.22) is integrated as

$$\begin{aligned} I_{FD}(z_R, z_S, r_0) =& \frac{r_0}{\sqrt{-c_2(r_0)}} \\ &\times \left[\pi - \sum_{i=S,R} \arcsin\left(1 + \frac{2c_2(r_0)}{c_1(r_0)} z_i\right)\right]. \end{aligned} \tag{B.25}$$

It follows that the arcsine term in Eq. (B.25) is well defined for the allowed region by Eq. (B.24), because

$$-1 \leq 1 + \frac{2c_2(r_0)}{c_1(r_0)} z_i < 1. \tag{B.26}$$

B.2.3 I_F in terms of b

In most of lens studies including References [5, 61], it is useful to express the deflection angle in terms of the impact parameter in stead to r_0, mainly because $b \sim D_L\theta$ for the lens distance D_L and the image angle direction θ.

Therefore, we look for an approximate expression of b. Near the PS, $c_1(r_0)$ and $b(r_0)$ are Taylor-expanded as

$$c_1(r_0) = \frac{C_m r_m D'_m}{B_m}(r_0 - r_m) + O((r_0 - r_m)^2), \tag{B.27}$$

$$b(r_0) = b_m + \frac{b_m D'_m}{4}(r_0 - r_m)^2 + O((r_0 - r_m)^3). \tag{B.28}$$

From Eq. (B.27), we find

$$r_0 < r_m, \tag{B.29}$$

where $c_1(r_0) > 0$ and $D'_m < 0$ are used. This inequality means that the light ray passes by the slight inside of the PS. This is because the PS is stable. This unusual behavior of the photon orbit implies also

$$b < b_m, \tag{B.30}$$

from Eq. (B.28). See Figure B.1 for the photon orbit behavior near the PS.

By combining Eqs. (B.27) and (B.28), we obtain, near the PS, an approximate relation between $c_1(r_0)$ and b as

$$c_1(r_0) \approx \frac{2 r_m C_m \sqrt{-D'_m}}{B_m}\left(1 - \frac{b}{b_m}\right)^{\frac{1}{2}}. \tag{B.31}$$

By substituting this into Eq. (B.25), we obtain

$$\begin{aligned} & I_{FD}(z_R, z_S, b) \\ & \simeq \frac{r_m}{\sqrt{-c_2(r_m)}} \\ & \times \left[\pi - \sum_{i=S,R} \arcsin\left\{1 - \frac{r_m\sqrt{-D'_m}}{2}\left(1 - \frac{b}{b_m}\right)^{-\frac{1}{2}} z_i\right\}\right]. \end{aligned} \tag{B.32}$$

By performing direct calculations for a photon traveling near the PS, we rearrange Eq. (B.24) as

$$0 < z_i \leq \frac{4}{r_m\sqrt{-D'_m}}\left(1 - \frac{b}{b_m}\right)^{1/2}, \tag{B.33}$$

for which the arcsine function in Eq. (B.32) is well defined.

In order to obtain Eq. (B.32) as an approximate estimation of I_F in terms of b, we have used the Taylor series expansion as Eq. (B.28), which is valid if

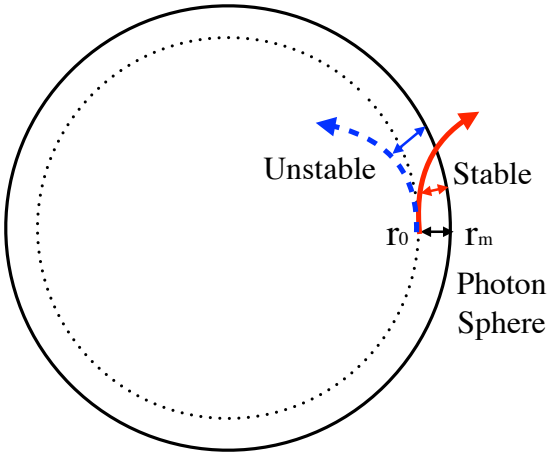

Figure B.1: Schematic figure of photon orbits near a PS. The PS is denoted by a solid circle with radius r_m. The dotted circle has radius r_0, which is slightly smaller than r_m. Namely, $r_m - r_0$ is taken as a perturbation around the PS. The initial position of the photon is r_0, at which the initial radial velocity is vanishing. The thick dashed blue (in color) arrow denotes a photon motion when the PS is unstable. The orbital deviation grows because of being unstable. Therefore, it is difficult for the inner photon to escape to a far region. This is why the earlier papers focused on $r_0 > r_m$ when an unstable PS is assumed [5, 61]. On the other hand, the thick solid red (in color) arrow denotes a photon motion when the PS is stable. The orbital deviation gets smaller because of being stable. It is thus possible that the inner photon ($r_0 < r_m$) crosses the PS to reach a distant observer.

$b_m > b_m|D_m^{'}|(r_0 - r_m)^2/4$. This requires that the closest approach of light and the PS are close enough to satisfy

$$|r_0 - r_m| < \frac{2}{\sqrt{|D_m^{'}|}}. \tag{B.34}$$

Yet, a lower bound on $|r_0 - r_m|$ exists in the neighborhood of the PS as shown below.

B.2.4 Discontinuity between the closest approach and the stable PS

Eq. (B.33) implies the existence of a gap between the allowed closest approach and the stable PS.

Proposition

In a SSS spacetime which possess a stable outer photon sphere, the closest approach of a photon from a source (or to a receiver) located at finite distance from the lens object is not allowed in the infinitesimal neighborhood of the stable PS.

Proof

This proposition can be proven by contradiction as follows. We consider a receiver (or a source) at finite distance from the lens, namely $r_i > r_0$, which leads to $z_i > 0$. We assume the closest approach of a photon orbit were in the infinitesimal neighborhood of the stable PS.

On the stable PS, $F_m = F_m^{'} = 0$, while $F_m^{''} < 0$. The last inequality comes from the unstable condition $D_m^{'} < 0$. The function F near the PS is thus Taylor-expanded as

$$F_0 = \frac{1}{2}F_m^{''}(r_0 - r_m)^2 + O\left((r_0 - r_m)^3\right). \tag{B.35}$$

From Eq. (B.9), H for $r_0 \approx r_m$ is expanded as

$$H = \frac{C_m F_m^{''}}{2B_m}(1-z)^4(r_0 - r_m)^2 + O\left((r_0 - r_m)^3\right), \tag{B.36}$$

where Eq. (B.35) is used.

By using $B_m > 0$, $C_m > 0$ and $F_m^{''} < 0$ for Eq. (B.36), we find $H < 0$ if $r_0 - r_m$ is sufficiently small. $H < 0$ contradicts with the existence of the photon orbit. The proof is completed.

The above proposition prohibits the closest approach in the infinitesimal neighborhood of the stable PS. However, it does not specify the size of the gap between

the allowed closest approach and the stable PS. To discuss the gap size, we use Eq. (B.33), which can be rewritten as

$$\frac{b}{b_m} \leq 1 - \frac{r_m^2 z_i^2 (-D_m^{'})}{16}. \tag{B.37}$$

Note that Eq. (B.33) is based on a quadratic approximation up to z^2.

For finite z_i and $D_m^{'} < 0$, Eq. (B.37) demonstrates that b is not allowed in the infinitesimal neighborhood of b_m. From Eq. (B.37), the upper bound on b is

$$b_{max} = b_m - \frac{b_m r_m^2 z_L^2 (-D_m^{'})}{16}. \tag{B.38}$$

Therefore, we obtain the gap size $\Delta b \equiv b_m - b_{max}$ is given by

$$\Delta b = \frac{b_m r_m^2 z_L^2 (-D_m^{'})}{16}, \tag{B.39}$$

where z_L is the larger of z_R and z_S, namely the value of z for the more distant one of the receiver and source.

A separate treatment is required for the marginal PSs ($D'_m = 0$) e.g. [10, 62].

B.2.5 The dominant part and the remainder

Before closing this section, we confirm that $I_{FR} \equiv I_F - I_{FD}$ is indeed the remainder. We can simply write it as

$$I_{FR}(z_R, z_S, r_0) \equiv \sum_{i=R,S} \int_0^{z_i} f_R(z, r_0) dz, \tag{B.40}$$

where $f_R(z, r_0) \equiv f(z, r_0) - f_D(z, r_0)$.

From Eq. (B.40), for $z_i < 1$,

$$I_{FR}(z_R, z_S, r_0) = \sum_{i=R,S} [f_R(z_i, r_0) z_i + O(z_i^2)]. \tag{B.41}$$

For $r_0 \sim r_m$, we have $f(z, r_m) \sim f_D(z, r_m)$ when $z < 1$. Thus, using the Taylor expansion method, one might assume that $f_R(z, r_m) = f(z, r_m) - f_D(z, r_m) = O(z)$. However, a more careful examination of the asymptotic expansion of $f_R(z, r_0)$ for $z < 1$ is needed [1]. By straightforward calculations, the

[1] There is a prohibited region around the stable PS as shown in Section B. 2. 4. Because the existence of this gap region, the functions H and f are not differentiable at $r = r_m$. As a result, H and f cannot be Taylor-expanded around r_m. In stead of Taylor expansions, therefore, we look for asymp- totic expansions of I_F, I_{FD} and I_{FR} through f, f_D and f_R.

asymptotic expansion of $f(z, r_0)$ for small z is obtained as

$$f(z, r_0) = \frac{r_0}{\sqrt{z c_1(r_0)}} - \frac{r_0 c_2(r_0)}{2 c_1(r_0)^{3/2}} \sqrt{z} + O(z^{3/2}). \tag{B.42}$$

Similarly, the asymptotic expansion of $f_D(z, r_0)$ is

$$f_D(z, r_0) = \frac{r_0}{\sqrt{z c_1(r_0)}} - \frac{r_0 c_2(r_0)}{2 c_1(r_0)^{3/2}} \sqrt{z} + O(z^{3/2}). \tag{B.43}$$

By comparing Eqs. (B.42) and (B.43), we find

$$f_R(z, r_0) = O(z^{3/2}). \tag{B.44}$$

Using this in Eq. (B.41), we obtain

$$I_{FR}(z_R, z_S, r_0) = O(z_R^{5/2}, z_S^{5/2}). \tag{B.45}$$

On the other hand, Eq. (B.25) is expanded, for small z_R and z_S, as

$$I_{FD}(z_R, z_S, r_0) = \frac{2 r_0}{\sqrt{c_1(r_0)}} (\sqrt{z_R} + \sqrt{z_S}) + O(z_R, z_S), \tag{B.46}$$

where we use $\arcsin(1 - \varepsilon) = \pi/2 - \sqrt{2\varepsilon} + O(\varepsilon)$.

For $z_R, z_S \ll 1$, Eqs. (B.45) and (B.46) lead to $I_{FR}(z_R, z_S, r_0) \ll I_{FD}(z_R, z_S, r_0)$. Therefore, we can safely conclude that I_{FD} is the dominant part and I_{FR} is the remainder.

B.3 Example: A class of Weyl gravity model

In the Weyl gravity model, Mannheim and Kazanas found a class of SSS solutions [41]. The metric reads

$$ds^2 = -g(r) dt^2 + g(r)^{-1} dr^2 + r^2 (d\theta^2 + \sin^2\theta d\phi^2), \tag{B.47}$$

where

$$g(r) = 1 - 3\beta\gamma - \frac{\beta(2 - 3\beta\gamma)}{r} + \gamma r - \kappa r^2, \tag{B.48}$$

and we consider $g(r) > 0$, namely the outside of the horizon.

The allowed region for the existence of the stable outer PS is [65]

$$\beta > 0, \tag{B.49}$$
$$\gamma < 0, \tag{B.50}$$
$$\kappa < 0. \tag{B.51}$$

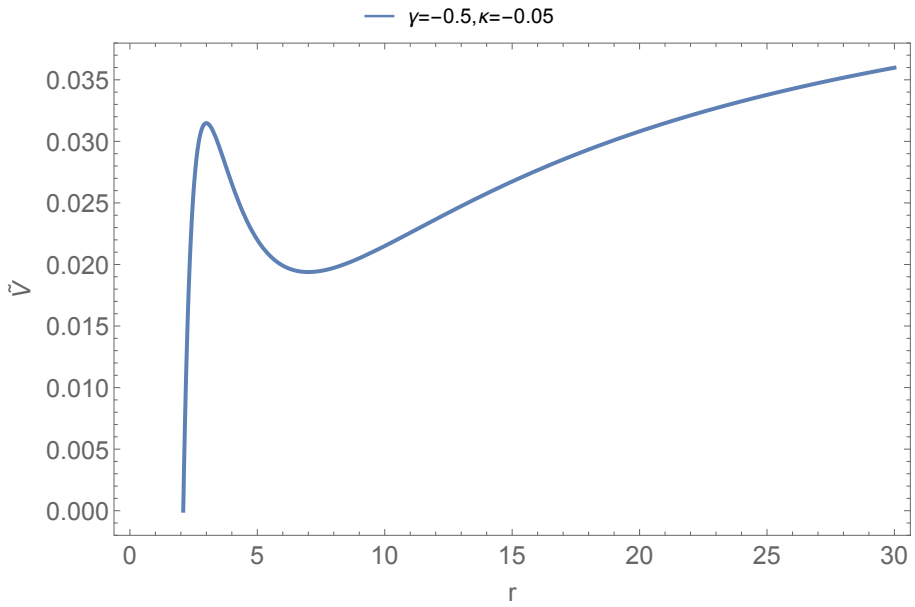

Figure B.2: Effective potential $\tilde{V}(r)$ in the Weyl gravity model. The solid blue (in color) curve corresponds to $\gamma = -0.5$ and $\kappa = -0.05$ in the unit of $\beta = 1$, which leads to the SOPS at $r_m = 7$. From $(b_m)^{-2} = \tilde{V}(r_m) = 0.0193878$, $b_m = 7.18184$ is obtained. $\tilde{V}(r)$ does not vanish for large r, because the spacetime is not asymptotically flat.

In this section, we focus on this parameter region.

We solve $D(r) = 0$ to find two roots as $r = 3\beta$ and $r = 3\beta - 2/\gamma$. They are corresponding to PSs. One is a stable PS and the other is an unstable one.

In the present case of $\gamma < 0$, the stable outer PS is located at

$$r_m = 3\beta - \frac{2}{\gamma}, \tag{B.52}$$

because

$$\begin{aligned} D'_m =& -\frac{2}{r_m^2 g(r_m)} \\ =& -\frac{2b_m^2}{r_m^4} \\ <& 0. \end{aligned} \tag{B.53}$$

The other root $r = 3\beta$ is the radius of the unstable inner PS.

Note that r_m is larger than 3β because of $\gamma < 0$. See Figure B.2 for the effective potential $V(r)$ in the Weyl gravity model with the stable outer PS.

There is a constraint on κ as [2]

$$\kappa < -\frac{\gamma^2(1-\beta\gamma)}{(2-3\beta\gamma)^2}. \tag{B.54}$$

Here, b_m denotes the critical impact parameter corresponding to the stable PS. It is obtained as

$$b_m = \frac{2-3\beta\gamma}{\sqrt{-\kappa(2-3\beta\gamma)^2 - \gamma^2(1-\beta\gamma)}}, \tag{B.55}$$

where the inside of the square root is always positive when κ satisfies Eq. (B.54).

From Eqs. (B.32) and (B.45), we obtain

$$\begin{aligned} &I_{FD}(z_S, z_R, b) \\ &\simeq \pi - \sum_{i=S,R} \arcsin\left\{1 - \frac{b_m}{\sqrt{2}r_m}\left(1 - \frac{b}{b_m}\right)^{-1/2} z_i\right\}, \end{aligned} \tag{B.56}$$

$$\begin{aligned} &I_{FR}(z_S, z_R, b) \\ &\simeq -\beta\gamma\left(\frac{b_m}{2\sqrt{2}r_m}\right)^{3/2}\left(1 - \frac{b}{b_m}\right)^{-3/4} \sum_{i=S,R} z_i^{5/2}, \end{aligned} \tag{B.57}$$

[2] Turner and Horne realized that a bound orbit of a photon is possible in this parameter region for the SSS solution in Weyl gravity [65].

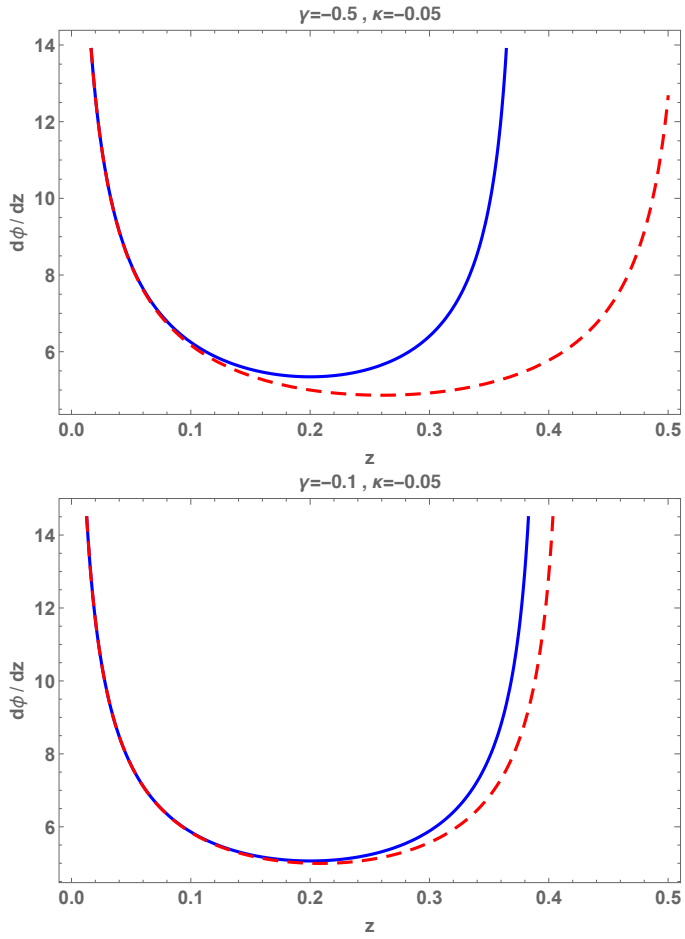

Figure B.3: The integrands of Eqs. (B.8) and (B.22). The solid blue (in clor) curve denotes f $(= d\phi/dz)$ in the integral I_F, while the dashed red (in color) curve denotes f_D in I_{FD}. The horizontal axis means z. We assume $\kappa = -0.05$ in the unit of $\beta = 1$ that is roughly corresponding to the conventional unit as mass $= 1$ in the Schwarzschild or Kottler spacetime. The top and bottom panels assume $\gamma = -0.5$ and $\gamma = -0.1$, respectively, each of which leads to $r_m = 7.0$ and $b_m = 7.18185$, and $r_m = 23$ and $b_m = 4.56815$, respectively. In both cases, the solid and dashed curves are overlapped better for smaller z. For instance, the difference between them is about 10 percents at $z \sim 0.2$. A significant deviation at large z is due to a departure from the quadratic approximation of $H(z)$ in z.

where straightforward calculations at $O(z^{5/2})$ are done in Eq. (B.45).

When $z_T \equiv z_R = z_S \ll (1 - b/b_m)^{1/2}$, Eq. (B.56) provides an approximate expression of the deflection angle as

$$\begin{aligned}\Delta\phi =& I_F \\ =& 2\sqrt{\frac{\sqrt{2}b_m}{r_m}\left(1-\frac{b}{b_m}\right)^{-1/2} z_T} \\ &+ O\left(\frac{b_m}{r_m}\left(1-\frac{b}{b_m}\right)^{-1/2} z_T\right).\end{aligned} \tag{B.58}$$

where we use $\arcsin(1-\varepsilon) = \pi/2 - \sqrt{2\varepsilon} + O(\varepsilon)$ for $\varepsilon < 1$.

It is natural that I_{FR} is much smaller than I_{FD}, as discussed in Section III. Eq. (B.56) shows the mild deflection in terms of the arcsine function. See Figure B.4 for a comparison of Eq. (B.56) and numerical calculations for I_{FD}. As shown in Figure B.3, f are dependent on rather strongly on γ. The difference between the numerical f and approximate one becomes significant as z is larger. On the other hand, the closest approach and its vicinity make a dominant contribution to the total angle integral I_F. In Figure B.4, therefore, I_F shows much weaker dependence on γ and z.

Finally, we discuss the gap size. By using Eq. (B.53) for Eq. (B.39), we obtain

$$\Delta b = \frac{b_m^3 z_L^2}{8 r_m^2}. \tag{B.59}$$

For $b_m \sim r_m$, furthermore, it becomes simply

$$\Delta b \approx \frac{1}{8} b_m z_L^2. \tag{B.60}$$

In a SSS spacetime, the PS was thought to be always an edge such as the inner boundary of a black hole shadow. However, Eqs. (B.59) and (B.60) provide a counterexample, when the PS is stable.

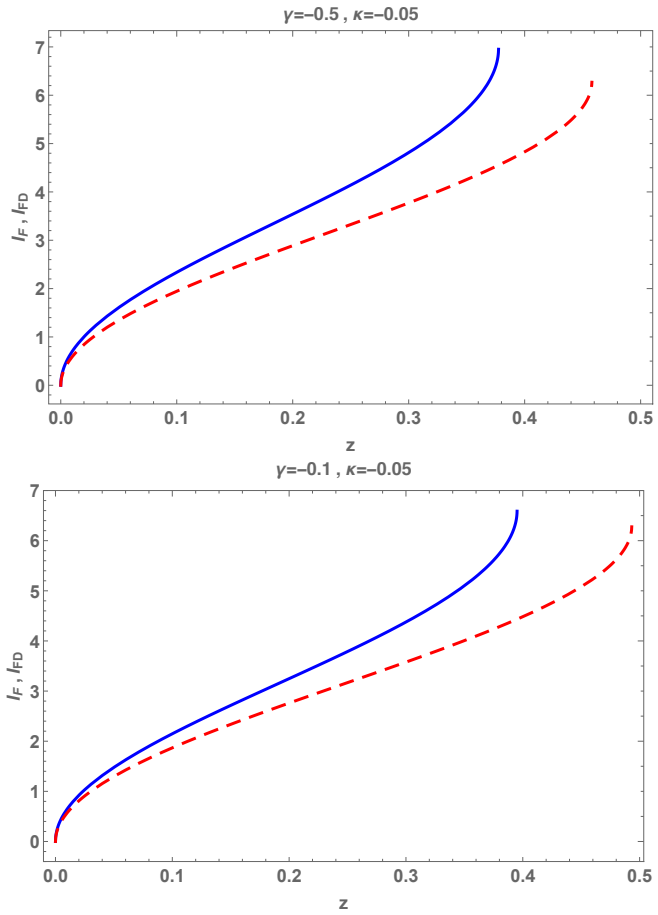

Figure B.4: The total angle integrals I_F and I_{FD}. The solid blue (in color) curve denotes the present approximation of I_{FD} by Eq. (B.56) and the dashed red (in color) curve denotes numerical calculations of I_F in Eq. (B.8), where we assume the same values for κ and γ in Figure B.3. For the simplicity, we choose $z \equiv z_R = z_S$, which is denoted by the horizontal axis. For $z \ll 1$, the two curves are very close to each other, because the quadratic approximation works well especially near $z \sim 0$. The two curves are close to each other especially for smaller z. For instance, the difference between them is roughly 20 percents at $z \sim 0.2$. A significant deviation at large z reflects a departure from the quadratic approximation of $H(z)$ in z.

References

[1] A. Addazi, A. Marciano, and N. Yunes, Eur. Phys. J. C **80**, 36 (2020).

[2] K. Akiyama et al. (Event Horizon Telescope Collaboration), Astrophys. J. **875**, L1 (2019); Astrophys. J. **875**, L2 (2019); Astrophys. J. **875**, L3 (2019); Astrophys. J. **875**, L4 (2019); Astrophys. J. **875**, L5 (2019); Astrophys. J. **875**, L6 (2019).

[3] K. Akiyama et al. (Event Horizon Telescope Collaboration), Astrophys. J. **930**, L12 (2022); Astrophys. J. **930**, L13 (2022); Astrophys. J. **930**, L14 (2022); Astrophys. J. **930**, L15 (2022); Astrophys. J. **930**, L16 (2022); Astrophys. J. **930**, L17 (2022).

[4] https://www.ngeht.org/

[5] V. Bozza, Phys. Rev. D **66**, 103001 (2002).

[6] V. Bozza, Phys. Rev. D **78**, 103005 (2008).

[7] V. Cardoso, L. C. B. Crispino, C. F. B. Macedo, H. Okawa, and P. Pani, Phys. Rev. D **90**, 044069 (2014).

[8] C. Cederbaum, and G. J. Galloway, Class. Quantum Grav. **33**, 075006 (2016).

[9] C. Cederbaum, and G. J. Galloway, J. Math. Phys. **62**, 032504 (2021).

[10] T. Chiba, and M. Kimura, Prog. Theor. Exp. Phys. **4**, 043E01 (2017).

[11] C. M. Claudel, K. S. Virbhadra, and G. F. R. Ellis, J. Math. Phys. **42**, 818 (2001).

[12] A. B. Congdon, and C. R. Keeton, *Principles of Gravitational Lensing* (Springer, NY, 2018).

[13] P. V. P. Cunha, E. Berti and C. A. R. Herdeiro, Phys. Rev. Lett. **119**, 251102 (2017).

[14] M. Cvetic, G. W. Gibbons, and C. N. Pope, Phys. Rev. D **94**, 106005 (2016).

[15] M. P. Dabrowski, and F. E. Schunck, Astrophys. J. **535**, 316 (2000).

[16] C. Darwin, Proc. R. Soc. A **249**, 180 (1959).

[17] Y. Decanini, A. Folacci, and B. Raffaelli, Phys. Rev. D **81**, 104039 (2010).

[18] S. Dodelson, *Gravitational Lensing* (Cambridge Univ. Press, NY, 2017).

[19] F. W. Dyson, A. S. Eddington, and C. Davidson, Phil. Trans. R. Soc. A **220**, 291 (1920).

[20] Q. Gan, P. Wang, H. Wu, and H. Yang, Phys. Rev. D **104**, 024003 (2021).

[21] R. Ghosh, and S. Sarkar, Phys. Rev. D **104**, 044019 (2021).

[22] G. W. Gibbons, and M. C. Werner, Class. Quant. Grav. **25**, 235009 (2008).

[23] G. W. Gibbons, and C. M. Warnick, Phys. Lett. B **763**, 169 (2016).

[24] S. Gillessen et al. Astrophys.J. **837**, 30 (2017).

[25] M. Guo, and S. Gao, Phys. Rev. D **103**, 104031 (2021).

[26] W. Hasse and V. Perlick, Gen. Rel. Grav. **34**, 415, (2002).

[27] S. Hod, Phys. Lett. B **727**, 345 (2013).

[28] S. Hod, Phys. Lett. **B** 776, 1 (2018).

[29] A. Ishihara, Y. Suzuki, T. Ono, T. Kitamura, and H. Asada, Phys. Rev. D **94**, 084015 (2016).

[30] A. Ishihara, Y. Suzuki, T. Ono, and H. Asada, Phys. Rev. D **95**, 044017 (2017).

[31] K. Izumi, Y. Tomikawa, T. Shiromizu, and H. Yoshino, Prog. Theor. Exp. Phys. **2021**, 083E02 (2021).

[32] J. Keir, Class. Quantum Grav. **33**, 135009 (2016).

[33] Y. Koga and T. Harada, Phys. Rev. D **94**, 044053 (2016).

[34] Y. Koga and T. Harada, Phys. Rev. D **98**, 024018 (2018).

[35] Y. Koga, Phys. Rev. D **99**, 064034 (2019).

[36] Y. Koga, Phys. Rev. D **101**, 104022 (2020).

[37] Y. Koga, T. Igata, and K. Nakashi, Phys. Rev. D **103**, 044003 (2021).

[38] R. A. Konoplya, and A. Zhidenko, Phys. Rev. D **103**, 104033 (2021).

[39] R. Kudo, and H. Asada, Phys. Rev. D **105**, 084014 (2022).

[40] R. Kudo, and H. Asada, Phys. Rev. D **111**, 044014 (2025).

[41] P. D. Mannheim, and D. Kazanas, Astrophys. J. **342**, 635 (1989).

[42] A. K. Mishra, S. Chakraborty, and S. Sarkar, Phys. Rev. D **99**, 104080 (2019).

[43] T. Ohgami, and N. Sakai, Phys. Rev. D **91**, 124020 (2015).

[44] H. C. Ohanian, Am. J. Phys. **55**, 428 (1987).

[45] T. Ono, A. Ishihara, and H. Asada, Phys. Rev. D **96**, 104037 (2017).

[46] T. Ono, and H. Asada, Universe, 5(11), 218 (2019).

[47] V. Perlick, Phys. Rev. D **69**, 064017 (2004).

[48] V. Perlick, Living Rev. Relativity **7**, 9 (2004).

[49] V. Perlick, and O. . Tsupko, Phys. Rep., **947**, 1 (2022).

[50] A. O. Petters, H. Levine, and J. Wambsganss, *Singularity Theory and Gravitational Lensing* (Springer, NY, 2012).

[51] N. G. Sanchez, Phys. Rev. D **18**, 1030 (1978).

[52] P. Schneider, J. Ehlers, and E. E. Falco, *Gravitational Lenses* (Springer, NY, 1992).

[53] T. Shiromizu, Y. Tomikawa, K. Izumi, and H. Yoshino, Prog. Theor. Exp. Phys. **2017**, 033E01 (2017).

[54] M. Siino, Class. Quantum Grav. **38**, 025005 (2021).

[55] M. Siino, ArXiv:2107.06551.

[56] I. Z. Stefanov, S. S. Yazadjiev, and G. G. Gyulchev, Phys. Rev. Lett. **104**, 251103 (2010).

[57] K. Takahashi, R. Kudo, K. Takizawa, and H. Asada Phys. Rev. D **108**, 124011(2023)

[58] K. Takizawa, and H. Asada, Phys. Rev. D **103**, 104039 (2021).

[59] K. Takizawa, T. Ono, and H. Asada, Phys. Rev. D **101**, 104032 (2020).

[60] K. Takizawa, T. Ono, and H. Asada, Phys. Rev. D **102**, 064060 (2020).

[61] N. Tsukamoto, Phys. Rev. D **95**, 064035 (2017).

[62] N. Tsukamoto, Phys. Rev. D **102**, 104029 (2020).

[63] N. Tsukamoto, Phys. Rev. D **104**, 064022 (2021).

[64] N. Tsukamoto, Phys. Rev. D. **104**, 124016 (2021).

[65] G. E. Turner, and K. Horne, Class. Quantum Grav. **37**, 095012 (2020).

[66] K. S. Virbhadra, and G. F. R. Ellis, Phys. Rev. D **62**, 084003 (2000).

[67] K. S. Virbhadra, Phys. Rev. D **106**, 064038 (2022).

[68] K. S. Virbhadra, Phys. Rev. D **109**, 124004 (2024).

[69] S. W. Wei, Y. X. Liu, and H. Guo, Phys. Rev. D **84**, 041501(R) (2011).

[70] C. M. Will, Living Rev. Relativity, **17**, 4 (2014).

[71] R. Yang, and H. Lu, Eur. Phys. J. C **80**, 949 (2020).

[72] H. Yoshino, K. Izumi, T. Shiromizu, and Y. Tomikawa, Prog. Theor. Exp. Phys. **2017**, 063E01 (2017).

[73] H. Yoshino, K. Izumi, T. Shiromizu, and Y. Tomikawa, Prog. Theor. Exp. Phys. **2020**, 023E02 (2020).

[74] H. Yoshino, K. Izumi, T. Shiromizu, and Y. Tomikawa, Prog. Theor. Exp. Phys. **2020**, 053E01 (2020).